Environmental evolution and geological significance of the Miocene carbonates of the Eratosthenes Seamount (ODP Leg 160)

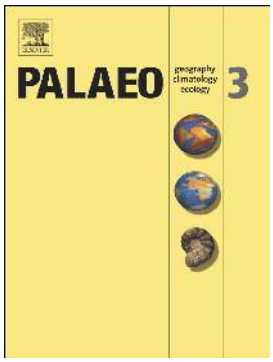

Environmental evolution and geological significance of the Miocene carbonates of the Eratosthenes Seamount (ODP Leg 160)

Giovanni Coletti, Daniela Basso, Christian Betzler, Alastair H.F. Robertson, Giulia Bosio, Akram El Kateb, Anneleen Foubert, Aaron Meilijson, Silvia Spezzaferri

PII: S0031-0182(18)30999-4
DOI: https://doi.org/10.1016/j.palaeo.2019.05.009
Reference: PALAEO 9187

To appear in: *Palaeogeography, Palaeoclimatology, Palaeoecology*

Received date: 29 November 2018
Revised date: 1 May 2019
Accepted date: 6 May 2019

Please cite this article as: G. Coletti, D. Basso, C. Betzler, et al., Environmental evolution and geological significance of the Miocene carbonates of the Eratosthenes Seamount (ODP Leg 160), Palaeogeography, Palaeoclimatology, Palaeoecology, https://doi.org/10.1016/j.palaeo.2019.05.009

Environmental evolution and geological significance of the Miocene carbonates of the Eratosthenes Seamount (ODP Leg 160)

Giovanni Coletti[1a]

Daniela Basso[1]

Christian Betzler[2]

Alastair H.F. Robertson[3]

Giulia Bosio[1]

Akram El Kateb[4]

Anneleen Foubert[4]

Aaron Meilijson[5]

Silvia Spezzaferri[4]

a: corresponding author, giovanni.p.m.coletti@gmail.com.

1: Department of Earth and Environmental Sciences of Milano-Bicocca University, Piazza della Scienza 4, 20126 Milano, Italy.

2: Institut für Geologie, Universität Hamburg, Bundesstrasse 55, 20146, Hamburg, Germany.

3: School of Geosciences, University of Edinburgh, Kings Buildings, West Mains Road, Edinburgh EH9 3JW, United Kingdom.

4: Department of Geosciences, Fribourg University, Chemin du Musée 6, 1700 Fribourg, Switzerland.

5: Dr. Moses Strauss Department of Marine Geosciences, Charney School of Marine Sciences, University of Haifa, Aba Khoushy Ave. 199, Mount Carmel, 3498838 Haifa, Israel.

Abstract

Miocene carbonates of the Eratosthenes Seamount, located offshore from Cyprus in the

Eastern Mediterranean (ODP Leg 160, Site 966), have been re-analysed. The use of SEDEX sequential extraction to evaluate the nutrient concentrations and of CT-Scan for the identification of large benthic foraminifera resulted in a more detailed palaeoenvironmental reconstruction and an improved stratigraphic framework. Three intervals are recognized in the succession and are attributed to the lower, middle and upper Miocene respectively. The lower Miocene interval is dominated by large benthic foraminifera and echinoids. This association colonized the top of the seamount following its uplift from deep-water to photic zone depth. The middle Miocene interval is characterised by rhodoliths and corals at its base and near the top, whereas seagrass/seaweed assemblages (with epiphytic foraminifera and hooked coralline-algal crusts) dominate its central part. The upper Miocene is represented by coral reef facies near its base and lagoonal facies toward its top. The succession deposited in an oligotrophic environment and exhibits a general shallowing-upward trend mainly controlled by tectonic activity related to the northward subduction of the African plate. The succession of the Eratosthenes Seamount is characterised by a diverse large benthic foraminifera assemblage in its lower part and by corals in its uppermost part, whereas corallines characterise the central interval. This trend is frequent in Miocene Mediterranean carbonates and its occurrence on an isolated seamount further proves its connection to the general evolution of the basin. The decline of miogypsinids and lepidocyclinids after the early Miocene is notable because the Eratosthenes was geographically close to the Indo-Pacific where both groups thrived also in the middle Miocene. This decline was probably caused by the early Miocene closure of the deep-water connection between the Indo-Pacific and the Mediterranean.

Key Words: Nutrients; CT-Scan; Large Benthic Foraminifera; Coralline Algae; Corals; Reefs.

1. Introduction

The Miocene is a key epoch in the history of Cenozoic cooling. This fundamental climatic shift dates back to the Eocene with the opening of the Drake Passage, thereby isolating Antarctica

from the other land masses (Lagabrielle et al., 2009). However, it was only after the Middle Miocene Climatic Optimum that the Antarctic Ice-sheets experienced a major expansion and the North Hemisphere Ice-sheets began to form (Larsen et al., 1994; Zachos et al., 2001; Shevenell et al., 2004; Lewis et al., 2007). While the Earth's climate was cooling, the (palaeo)Mediterranean basin was changing from a large seaway connecting the Indo-Pacific with the Atlantic to an enclosed basin (Fig. 1; Dercourt et al. 2000). The eastern, deep-water oceanic connection was severed around the end of the early Miocene (Fig. 1A; Aktaş and Robertson, 1984; Yılmaz, 1993; Robertson, 1998e; Rögl, 1999; Dercourt et al., 2000; Taylforth et al., 2014). Despite this, shallow-marine seaways survived until the Serravallian as indicated by the presence of shallow water carbonates and evaporites in the Mesopotamian Basin (i.e. the area of present day Syria and Iraq; Buchbinder, 1996a; Rögl, 1999; Perrin and Bosellini, 2012; Taylforth et al., 2014; BouDagher-Fadel, 2018). During the late Miocene, the western passage was sealed resulting into the Messinian Salinity Crisis (Fig. 1B; Hsü et al., 1973; Adams et al., 1977; Dercourt et al., 2000).

Until the early Miocene the Eastern Mediterranean basin was the only gateway to the Indo-Pacific Ocean, and therefore plays a key role in the environmental evolution of the Mediterranean. Recent hydrocarbon discoveries (e.g. Tamar, Leviathan, Aphrodite and Zohr fields) have increased the international interest in this region (Peck, 2008; Skiple et al., 2012; Marlow, 2014; Montadert et al., 2014; Papadimitriou et al., 2018). The geological development of the Eastern Mediterranean, including its palaeoceanography, has been mainly controlled by relative movements of the Eurasian, Arabian and African plates (Robertson and Dixon, 1984; Robertson, 1998e). Microplate interaction adds complexity to this region (Mascle et al., 2000; Robertson et al., 2012, 2013; Montadert et al., 2014). Carbonate deposits are useful instrument to study the evolution of a basin because they record climatic and oceanographic variations, including sea-level oscillations. During the early Miocene, in the Eastern Mediterranean, fine-grained siliciclastic deposition prevailed near the Levantine coast, probably due to high fluvial influx from the African continent. Substantial carbonate production was only possible well away from major rivers (Buchbinder, 1996a, b). The

Miocene carbonate succession of the Eratosthenes Seamount south of Cyprus (Mart and Robertson, 1998) is therefore of particular interest. The seamount represents the topographically highest preserved elevation of the Eratosthenes Continental Block, that was detached from the North African-Arabian margin by rifting during the Mesozoic (Fig. 2A, B; Mart and Robertson, 1998; Robertson, 1998a, b, f; Mascle et al., 2000; Skyple et al., 2012; Montadert et al., 2014). Miocene shallow-water carbonates developed on the crest of this structure isolated from terrestrial influx, recording both the oceanographic and the tectonic evolution of the region (Fig. 2C; Robertson et al., 1995; Major et al., 1998; Mart and Robertson, 1998; Robertson, 1998b, c; Montadert et al., 2014). The focus of this work is to understand better the palaeoenvironmental evolution of these carbonates, particularly the nutrient availability which has been studied with the SEDEX sequential extraction. This technique allows a quantification of the bioavailable phosphorus in the palaeoenvironment, which represents the main limiting nutrient over the long timescale (Tyrrell, 1999). In addition, the stratigraphy of the Miocene succession is refined, based on foraminifera distribution (in particular large benthic foraminifera) and Sr isotope analysis.

2. Geological setting

2.1. The Mesozoic

The Eratosthenes Continental Block was detached in the Triassic from the Northern African-Arabian margin by a rifting phase that led to the opening of a southerly strand of the Neotethys (Robertson, 1998e; Garfunkel, 2004; Peck, 2008; Marlow, 2014; Montadert et al., 2014; Feld et al., 2017). Its basement is likely to be composed of thinned continental crust with mafic intrusions or other volcanics related to the rifting (Robertson, 1998e, f; Ben-Avraham et al., 2002; Montadert et al., 2014). Further extension and spreading occurred along the margin during the Jurassic and the Early Cretaceous (Gardosh et al., 2010; Skiple et al., 2012; Montadert et al., 2014). Following rifting and rift-related volcanism, the Eratosthenes Continental Block became a site of shallow-water carbonate production (Robertson, 1998e; Montadert et al., 2014; Papadimitriou et al., 2018).

During ODP Leg 160 the Eratosthenes Seamount was investigated via the drilling of three holes (ODP Sites 965, 966, 967; Fig. 2B, C), of which Site 967 penetrated as far as a Mesozoic carbonate succession (Fig. 2C; Emeis et al., 1996; Robertson, 1998a, e). Above a fractured limestone unit, Cretaceous (Aptian or older) neritic limestone was recovered in ODP Hole 967E (Fig. 3; Premoli-Silva et al., 1998; Robertson, 1998a). This shallow-water carbonate unit contains micritic intraclasts, pellets, benthic foraminifera, calcareous algae, molluscs, and other skeletal grains (Premoli-Silva et al., 1998; Robertson, 1998a). This assemblage formed within the photic zone and suggests a low energy environment, interpreted as a lagoon (Premoli-Silva et al., 1998; Robertson, 1998a). These shallow-water carbonates are overlain by laminated, locally bioturbated, pelagic chalk with planktonic foraminifera and rare echinoid fragments (Fig. 3; Robertson, 1998a). Several organic-rich layers occur within the chalk (Robertson, 1998a). Pelagic carbonate sedimentation probably began during the Cenomanian and continued until the Maastrichtian, with a hiatus in the Turonian (Premoli-Silva et al., 1998; Robertson, 1998a, f). The pelagic carbonate accumulated in a quiet, deep-water environment that was generally well-oxygenated and periodically current-winnowed. The organic-rich intervals may be related to periods of reduced circulation (or increased regional productivity; Meilijson et al., 2015), leading to reduced oxygen availability at the seafloor (Robertson, 1998a, f). The lack of gravity deposits is consistent with deposition on a isolated submerged platform, suggesting that the Eratosthenes Seamount was still located well away from the northern active plate margin where it is today (Robertson, 1998a, f). A similar late Cretaceous deepening is recorded along the Levantine margin and also in Southern Turkey (Robertson, 1998a, d, e; Meilijson et al. 2014; Papadimitriou et al., 2018). However, the exact timing of the deepening could be diachronous in the different areas (Robertson, 1998a; Montadert et al., 2014).

2.2 The Cenozoic

Paleogene planktonic foraminifer chalks were recovered at both ODP Sites 966 and 967 (Figs 2, 3; Premoli-Silva et al., 1998; Robertson, 1998a, f; Staerker, 1998). Pelagic sedimentation is

recorded up to the Oligocene (probably lower Oligocene, Premoli-Silva et al., 1998) at Site 967 and up to the upper Bartonian at Site 966 (Unit IV; Fig. 3; Staerker, 1998). In Hole 966F a major hiatus separates Eocene chalk (Unit IV; Fig. 3) from the overlying, coarse-grained, bioclastic, Miocene limestones (Unit III; Fig. 3). This hiatus is indicated by abundant glaucony, suggesting a prolonged period of reduced sedimentation or non-deposition (Major et al., 1998; Robertson, 1998a, b). The Miocene limestones are generally pure carbonates consisting of calcite and dolomite, as expected for an isolated platform (Robertson, 1998b). They are mainly composed of coralline algae, hermatypic corals and large benthic foraminifera, and were formed in a shallow-water environment within the photic zone (Emeis et al., 1996; Major et al., 1998; Robertson, 1998b). Two sub-units are recognised. The lower one (IIIb; Fig. 3) is rich in foraminifera and is characterised by relatively uniform physical properties (Emeis et al., 1996; Major et al. 1998). The upper one (IIIa; Fig. 3) is rich in calcareous algae and corals and has more variable physical properties (Emeis et al., 1996; Major et al. 1998). Miocene shallow-water limestones, dominated by algae and corals, also occur at ODP Site 965, whereas no shallow-water carbonates were recovered at ODP Site 967 (Fig. 3; Major et al., 1998). At ODP Site 965 Sr isotope analysis suggests that at least part of the succession is Tortonian (Major et al., 1998; Robertson 1998b).

At the end of the Miocene, during the Messinian Salinity Crisis, the Eratosthenes emerged, as indicated by the presence at ODP Sites 965 and 966 of paleosols and breccias, produced by sub-aerial weathering and fault activity (Unit II; Fig. 3; Major et al., 1998; Major and Ryan 1999; Robertson, 1998c, e, f). In contrast, brackish-water associations (*Cyprideis pannonica* and other brackish ostracodes) were recovered at ODP Site 967 (Spezzaferri et al., 1998). Zanclean deep-water sediments and sapropels overlay Messinian deposits at all sites as consequence of the early Pliocene re-establishment of open marine conditions in the Mediterranean (Unit I; Fig. 3; Major et al., 1998; Robertson, 1998c, e, d, f; Spezzaferri and Tamburini, 2007).

2.3 Cenozoic tectonics

The pronounced change in sedimentation between the Paleogene and the Neogene is related to uplift of the Eratosthenes Seamount from deeper water to at least photic-zone depths (Emeis et al., 1996; Robertson, 1998b, d, e, f; Whiting, 1998). The lack of erosion of the underlying chalk, and of sub-aerial weathering (e.g. karst formation), suggests that the uplift was not associated with sub-aerial exposure (Robertson, 1998f). The uplift was probably tectonically controlled and can be related to the northward subduction of the African Plate beneath Eurasia (Robertson, 1998f; Kinnaird and Robertson, 2013; Feld et al., 2017). Uplift and a transition from pelagic to shallow-water sedimentation are actually also recorded locally on Cyprus (Robertson et al., 1991; Eaton and Robertson, 1993; Major et al., 1998; Robertson, 1998b, c, d, e, f; BouDagher-Fadel and Lord, 2006; Kinnaird and Robertson, 2013). The northward subduction is also connected, via slab rollback, to the opening of the Cilicia Basin north of Cyprus (Mart and Ryan, 2002). The subsequent change from Miocene shallow-water carbonates to deeper-water Pliocene sediments suggests that the Eratosthenes Seamount underwent significant subsidence during the Messinian – early Pliocene time interval (Robertson 1998c; Major and Ryan 1999). Deepening upward is also recorded by the benthic foraminiferal assemblage within the overlying Plio-Pleistocene succession (Robertson, 1998d, f; Spezzaferri and Tamburini, 2007). This subsidence is explained by collision and underthrusting of the Eratosthenes Seamount beneath Cyprus and is coupled with a strong uplift of the island (Robertson et al., 1991; Robertson, 1998c, e, f; Kinnaird et al., 2011; Kinnaird and Robertson, 2013; Feld et al., 2017). Loading by the thick evaporites surrounding the Eratosthenes also contributed to this subsidence (Major et al., 1998; Major and Ryan, 1999). After the collision of the Eratosthenes Seamount with the Cyprus active margin, the fast westward migration of Anatolia become the main control on the region, inducing significant strike-slip motion along the lineaments of the Cyprus Arc (Mart and Ryan, 2002; Robertson et al., 2012; Kinnaird and Robertson, 2013).

3. Material and methods

ODP Hole 966F was chosen for this research because the entire Miocene carbonate succession was recovered within it (Unit III; Fig. 3; Major et al., 1998), including its lower contact with the underlying Eocene chalk (Unit IV; Fig. 3; Major et al., 1998). Also the recovery is less affected by diagenesis than in ODP Site 965 (Robertson, 1998b). Macroscopic and microscopic examinations of the cores were performed at MARUM – IODP Core Repository in Bremen (Germany), to observe the distribution of large bioclastic components and the average grain-size. Representative samples of the limestones were collected (Table S1) and 50 thin sections (polished with 1 μm aluminum oxide) were prepared. The petrographic characteristics and the skeletal assemblages of the limestones were studied in thin sections with the point-counting technique, using a 200 μm mesh and counting more than 500 points in each section (Flügel, 2010). To avoid oversampling of large elements, 6 randomly selected fields, with no overlap between them, were analysed for each section. At least 90 points were counted in each field. Following Odin and Letolle (1980), Odin and Matter (1981) and Amorosi (1995, 1997), the glauconitic grains have been collectively defined as glaucony (glauconite is used only for the K-rich end member of the glauconitic mineral family). The glaucony grains were divided into nascent, slightly evolved, evolved and highly evolved on the basis of their mineralogical maturity which reflects the time of residence at the water-sediment interface (Odin and Matter, 1981; Amorosi, 1997). Particular attention was paid to the foraminiferal assemblages including their taxonomic composition and the dominant groups. These features were assessed via observation of the whole thin section rather then with point-counting, in order to avoid overestimating large specimens. Coralline algae distribution and their taxa were considered at suprageneric level. The high-rank taxonomy follows Woelkerling (1988), adapted to the palaeontological use by Braga et al. (1993) and later modified by Harvey et al. (2003), Le Gall et al. (2009), Nelson et al. (2015) and Rösler et al. (2016).

The studied succession of ODP Hole 966F is rich in large benthic foraminifera (LBF). However, the deposits are strongly lithified and, therefore, LBF cannot be extracted to make orientated thin sections which are very important for reliable taxonomic identification (Briguglio et

al., 2013, 2014). The limited amount of recovered material makes the preparation even more challenging. To overcome both problems, we used X-ray Computed Tomographic Scanning techniques (CT-scan) for the non-destructive analysis of three samples rich in LBF (core 23R-1, cm 57 to 53, core 19R-2 cm 129 to 125; core 19R-2 cm 75 to 80). Small, hand-made, cylindrical sub-samples ($r < 1$ cm) of limestone were prepared and scanned at the University of Fribourg (Switzerland) using the multi-scaled Bruker X-ray Nano CT-scan system SkyScan 2211, with an X-ray source with a diamond-window target at energies of 80 kV, currents of 510 µA and applying a 0.5 mm titanium filter. Images were acquired on a Flat-Panel detector resulting in a voxel resolution of 7 µm. 360° scans were performed with a rotation step of 0.1°. The images were subsequently reconstructed with InstaRecon applying Gaussian smoothing, beam hardening and ring artefact corrections. The 3D models of the samples were sub-divided into smaller volumes of interest, each including a single specimen. These models were studied following the approach proposed by Coletti et al. (2018b). The identification of the LBF was based on the biometric characteristics of equatorial sections, integrating different procedures and various biometric parameters proposed in the literature (Fig. 4; Tan, 1932; Drooger and Socin, 1959; Van der Vlerk, 1959, 1963; Amato and Drooger, 1969; Matteucci and Schiavinotto, 1977; Schiavinotto, 1979; Chaproniere, 1980; Drooger, 1993; Verrubbi and Schiavinotto, 2005; Özcan et al., 2009; Hohenegger, 2011; Benedetti et al., 2017; Torres-Silva et al., 2017; Briguglio, 2018). Following Özcan et al. (2009) the notation exemplum intercentrale was used whenever the mean value of the identifying parameter of a group of specimens fell very close to the limits of two contiguous species of the same lineage. The biostratigraphic framework, based on the distribution of LBF, was integrated with the distribution of planktonic foraminifera.

To further support the biostratigraphic framework, Sr isotope analyses were performed. Suitable bivalves for Sr isotope analyses -sufficiently large and lacking evidence of dissolution with optical microscope, Scanning Electron Microscope (SEM) and Raman spectroscopy- were identified only in core 10R-2. Sampling was performed with a Dremel microdriller and ca. 10 mg of

powder was obtained for each sample. Trace elements (to further assess the preservation) were measured through Inductively Coupled Plasma Optical Emission Spectrometry (ICP-OES), Sr isotope analyses using a Finnigan MAT 262 multicollector mass spectrometer. Both analyses were performed at Ruhr-Universität in Bochum (Germany). Final ages were calculated with the LOWESS 5 table for the GTS2012 timescale (McArthur et al., 2012).

Twenty-eight samples, representative of the major variations observed in the hole, were analysed using the SEDEX sequential extraction method (replicas were made for 14 samples in order to check the repeatability of the analyses). SEDEX extraction allows an accurate quantification of the five known sedimentary phosphorus reservoirs (Ruttenberg, 1992, 2004; Ruttenberg et al., 2009); i.e. loosely-bound phosphorus; Fe-bound phosphorus; authigenic phosphorus (carbonate-fluoroapatite, biogenic apatite and carbonate bound phosphorus); detrital apatite and organic phosphorus (Ruttenberg, 2004). Except for detrital apatite, all these are sinks for reactive P present in the sea-water (Ruttenberg, 1992). The sum of their contribution (bioavailable-P) is related to the nutrient concentration in the palaeoenvironment at the time of sediment formation (Coletti et al., 2017). The samples were ground using a Dremel microdriller and then sieved through a 125 μm mesh (Ruttenberg et al., 2009). For each sample, 80 mg of the sieved sediment were analysed through the sequential extraction line set-up at the University of Fribourg in Switzerland using the method of Stalder et al. (2014).

Since core recovery was poor in the investigated interval of the core (15-20% on average in Unit III), the information resulting from the analyses were integrated with the available downhole logging data acquired during Leg 160 (Emeis et al., 1996; Major et al., 1998).

4. Results

4.1 Facies description

4.1.1 Cores 26R-1 to 20R, grainstone, LBF and echinoid facies

The contact between the pelagic, organic-rich Eocene chalk (Unit IV; Fig. 5) and the

overlying Miocene coarse shallow-water limestones (Unit III; Table 1; Fig. 5) is sharp. Large grains (several mm across) of glaucony occur just above the boundary. The size of the glaucony grains decreases rapidly upcore. Millimeter-sized specimens of lepidocyclinids are visible under the microscope. Upwards (core 25R), glaucony almost disappears whereas both the macroscopic and microscopic features of the limestone remain similar. Lepidocyclinids and other LBF are visible in hand specimens until core 20R (Fig. 5).

Thin section analysis reveals that in the basal part of this interval (26R-1) the skeletal assemblage is dominated by echinoid fragments, planktonic and benthic foraminifera (Table 1; Figs 5, 6A). Bryozoans, coralline algae and molluscs are minor components (Fig. 5). Glaucony is common, the grains are highly evolved and deep green, either small rounded or extremely large (Fig. 6A, B). Glauconized planktonic foraminifera occur within these large grains (Fig. 6B). The foraminiferal assemblage is dominated by planktonic species together with large thin lepidocyclinds and common small rotaliids. The overlying core 25R is similar, but only small grains of evolved glaucony are present and foraminifera, both planktonic and benthonic, are slightly more abundant (Fig. 5). Planktonic foraminifera dominate the assemblage in core 25R together with *Miogypsina* and *Nephrolepidina*. The skeletal and foraminiferal assemblages of cores 24R to 21R are dominated by LBF (Figs 5, 6C-E). The most common genera are *Miogypsina* (especially in 23R; Fig. 6C) and *Nephrolepidina* (especially in 21R; Fig. 6E). *Amphistegina,* mainly represented by relatively thick specimens (thickness/diameter ratio, T/D, between 0.4 and 0.5), and *Operculina* are less common (Fig. 6D). Echinoids and small rotaliids are abundant, whereas planktonic foraminifera are rarer (Fig. 5). Coralline algae are a minor component of the skeletal assemblage (common only at the top of 20R), and bryozoans are very rare. Glaucony is rare, the grains are small but very green (evolved). Although bioclasts in core 26R to 21R are relatively well preserved, the top of core 20R is recrystallized.

4.1.2 Core 19R-3, rudstone, rhodolith and coral facies

The limestone is very coarse-grained with common centimetre-sized rhodoliths (Figs 5, 7A). The coralline algae composing the rhodoliths are mainly Corallinales and Sporolithales. Fragments of corals (probably *Porites*) also occur, especially near the top of the section (Fig. 5).

Thin sections analysis shows that although coralline algae dominate the skeletal assemblage, corals and benthic foraminifera are also important (Table 1; Fig. 5). The foraminiferal assemblage includes thick specimens of *Amphistegina* (T/D between 0.5 and 0.6), small benthics and rare *Heterostegina.* Coralline algae of the order Hapalidiales were also observed in the thin sections.

4.1.3 Cores 19R-2 to 16R-2, wackestone to packstone, coralline algal and *Heterostegina* facies

The lower part of this facies (cores 19R-2 and 19R-1) is much more fine-grained than the underlying rhodolith and coral rudstone, and contains common *Heterostegina*, generally 1 mm thick and up to over 1 centimeter in diameter (T/D between 0.1 and 0.15; Figs 5, 7B). The orientation of the tests ranges from perpendicular to the drilling direction, to randomly oriented. Very thin, disarticulated bivalves also occur. Hooked crusts of coralline algae are common, especially from 19R-1 upcore (Fig. 5). Core 19R-1 includes centimetre-sized burrows (Fig. 7C). From cores 18R to 17R-4, coralline algae and LBF still dominate, but rhodoliths with laminar structure and small coralline branches become more common, especially toward the top of the interval. *Heterostegina* specimens, although still very large and flat, are slightly thicker (T/D between 0.1 and 0.2) than those of cores 19R-1 and 19R-2. Locally they have dissolved leaving only moldic porosity. Upwards (cores 17R-3 to 16R-2), coralline algae clearly dominates the core whereas *Heterostegina* become rare (Fig. 5). Coralline branches and rhodoliths become particularly common, the latter especially so in core 16R. Hooked crusts remain widespread (Fig. 7D). At the contact between 16R-2 and 16R-3, the extensive presence of Corallinales-dominated large algal structures (larger than the diameter of the core) may represent very large rhodoliths or a coralline bioconstruction.

Based on thin section analysis, the lower part of the facies (cores 19R-2 to 18R-1) is largely dominated by coralline algae and benthic foraminifera (Table 1; Fig. 5). The foraminiferal

assemblage is dominated by *Neoconorbina* (Fig. 6F, G) and *Heterostegina* (Fig. 6H). *Amphistegina*, *Operculina*, *Cibicides*, *Elphidium*, and textulariids are rare. Coralline algae mostly consist of thin and sometimes fragmented crusts (Fig. 6I) and small branches of Hapalidiales (Fig. 6H). Bivalve shells are locally abundant. Echinoid fragments and planktonic foraminifera (including *Orbulina universa*) were also noted (Fig. 5). Bioclasts in this interval are moderately well preserved; however, the muddy matrix in which they are embedded is often recrystallized, with rhombohedral crystals of dolomite (Fig. 6I). Recrystallization is locally more intense (e.g. 18R-2; Fig. 6J). Dissolution and recrystallization are pervasive upward (cores 17R – 16R; Fig 6K), and only coralline algae are preserved (Fig. 5).

4.1.4 Cores 16R-1 to 15R-1, rudstone, rhodolith and corals facies

This facies is dominated by rhodoliths. Fragments of colonial coral (probably *Porites*) also occur (Fig. 5). Although some rhodoliths are branched (Fig. 7E), others have a compact laminar structure. Hooked crusts and *Heterostegina* molds are very rare. The rhodoliths are dominated by Sporolithales and Corallines.

In thin section the rock is mainly recrystallized. What little can be seen of the skeletal assemblage is coralline algae (mostly Sporolithales), colonial corals and benthic foraminifera, mainly *Amphistegina* and small benthic rotaliids (Table 1; Figs 5, 6L). Due to the poor preservation, the T/D ratio of the specimens of *Amphistegina* of this facies was not evaluated.

4.1.5 Cores 15R-1 to 14R-1, recrystallized layer

This interval is largely recrystallized with abundant moldic porosity related to the dissolution of various bioclasts, including bivalves. There are no preserved skeletal grains and the limestone is almost entirely composed by rhombohedral carbonate crystals (Fig. 5).

4.1.6 Cores 14R-1 to 11R, rudstone/boundstone, coral-reef facies

The interval from cores 14R-1 to 11R is very coarse and is clearly dominated by colonial corals (Table 1; Fig. 5). The latter are especially abundant in 13R-1, 12R-2 and 11R-1. Most of the large coral fragments are poritids, but some could be probably attributed to *Tarbellastrea* due to the small but well defined corallites (Fig. 7F). Coralline algae are also common, occurring as branches and as small compact rhodoliths. Large echinoid spines are locally abundant.

In thin section the skeletal assemblage is dominated by corals and coralline algae, with important contributions from benthic foraminifera (Table 1; Fig. 5). Molluscs and echinoids are locally abundant (Fig. 5). Toward the top of this interval (11R-1), the abundance of benthic foraminifera and molluscs increases, and the preservation improves (Fig. 5). The foraminiferal assemblage is dominated by miliolids, including *Borelis melo melo* and *Dendritina;* encrusting foraminifera are also common (Fig. 5). Most of the observed coralline algae are Corallinales (among them abundant *Titanoderma*). Scarce Sporolithales also occur.

4.1.7 Cores 10R to 7R-1, grainstone to packstone, mollusc and benthic foraminifer facies

In the lower part of this interval (core 10R), the limestone is very coarse-grained with common molluscs and coralline algae (Table 1; Fig. 5). The core shows low-porosity, well-cemented layers with common and well-preserved bivalves (Fig. 7G), alternating with layers in which the shells are mostly dissolved resulting in high moldic-porosity. Coralline algae are present as branches and small rhodoliths. Corals also occur and are locally abundant. Abundant large miliolids (Fig. 7H) and also coated grains built by encrusting foraminifera can be observed in the highly cemented layers. Near the top of core 10R, there are also small fragments of vermetid encrustations. Upwards (core 9R), the rock is similar but grain-size decreases. In core 8R and in most of core 7R the limestone is even finer grained and is characterised by high moldic porosity (dissolved molluscs, both bivalves and gastropods; Fig. 5).

Thin section analysis shows that benthic foraminifera (predominantly small miliolids, *B.*

melo melo, *Dendritina* and encrusting rotaliids; Fig. 6M) and molluscs (Fig. 6N) dominate the skeletal assemblage (Table 1; Fig. 5). Coralline algae (mostly Corallinales) and coral fragments are locally abundant, especially in core 10R (Fig. 6O). The well cemented layers of core 10R present two generations of cement: an isopachous fibrous cement enveloping skeletal grains and a sparitic cement filling most of the inter-grain porosity (Fig. 6N). In these layers skeletal grains which are generally sensitive to dissolution, like the green calcareous alga *Halimeda* (Fig. 6P), are preserved. In the upper part of the interval (8R and 7R-1), the deposits are mud-supported, with more small miliolids and ostracods and less coralline algae and corals (Table 1; Figs 5, 6Q).

4.1.8 Core 7R-1, packstone, mollusc and ostracod facies

A chaotic layer with limestone fragments embedded in a gray muddy matrix occupies the central part of 7R-1. This layer belongs to the breccia unit (Unit II; Figs 3, 5), that is located above the Miocene shallow-water limestone and represents the upper boundary of the investigated succession. At the top of 7R-1, there is a lithified limestone interval with well developed moldic porosity, created by bivalve shell dissolution. Its skeletal assemblage is dominated by ostracods and small benthic foraminifera together with partially dissolved bivalves (Table 1; Figs 5, 6R).

4.2 SEDEX sequential extractions

The determined bioavailable-P concentrations are relatively uniform and very low in the Miocene cores (Unit III; Fig. 8). The only exception is core 23R, which contains authigenic minerals, as indicated by facies analyses (Fig. 8). Samples from the units above and below the marine Miocene shallow-water limestones (Units II and IV; Fig. 8) stand out clearly since they have remarkably higher concentrations of bioavailable-P (Fig. 8). There is no evidence of changes in bioavailable-P concentrations related to the different diagenetic patterns present into the core (Figs 5, 8). No differences were observed between replicas and original analysis indicating good

repeatability.

4.3 Stratigraphy

The assemblage of core 26R includes only lepidocyclinids, while the LBF assemblage of cores 25R to 21R is characterised by *Miogypsina*, *Nephrolepidina* and an absence of *Miogypsinoides* (Fig. 6C, D, E). The assemblage suggests an early Miocene age (Cahuzac and Poignant, 1997). Species were identified in core 23R using the CT-scan. The examined sample of miogypsinids (17 individuals) exhibits an unimodal distribution of the protoconch size and rather constant biometric parameters, suggesting that it consists of a single species. The biometric parameters of the *Miogypsina* specimens encompass the morphometric transition between *Miogypsina globulina* and *Miogypsina intermedia* (PW = 150 μm; DW = 170 μm; PS = 145 μm; DR = 1,2; X = 5.5; λ = 4°; V = 48; Fig. 9A). The only three lepidocyclinids observed were identified as *Nephrolepidina tourneri* (PW = 260 μm; DW = 410 μm; PS = 210 μm; DR = 1.65; Ai = 52%; NACII = 6; Fig. 9B, C). Thanks to the CT-scan, it was also possible to identify *Miolepidocyclina* in the association. The occurrences of *M.* exemplum intercentrale *globulina-intermedia* together with *N. tourneri* indicate a Burdigalian age for core 23R (Cahuzac and Poignant, 1997; Özcan and Less, 2009; Özcan et al., 2009; BouDagher-Fadel and Price, 2010, 2013). Above the core 20R, according to CT-scan and thin section investigations, miogipsinids and lepidocylinids entirely disappear. Heterosteginids are common in the interval between cores 19R-2 and 16R-2. The heterosteginds of core 19R-2 studied with the CT-scan (13 individuals) have an unimodal distribution of PS, suggesting the presence of a single species. Their biometric parameters (PW = 200; DW = 275; PS = 190; DR = 1.35; OC = 1.5; S3+4 = 2.5; S4+5 = 3.5; NC1 = 10; D1 = 1220; Fig. 9D, E) suggest a taxonomic assignment close to *Heterostegina papyracea* (as described by Papazzoni and Sirotti, 1999) and “morphotype a” of *Heterostegina gomez-angulensis* (as described by Tosquella et al., 2001). From the core 14R upwards the succession is characterised by

the presence of *B. melo melo* (Fig. 9H) often associated with *Dendritina*. The occurrence of *Heterostegina* and *B. melo melo* together with the absence of lepidocyclinids and miogypsinids suggest that, upcore from 20R, the sediments are of middle or late Miocene (Betzler and Schmitz, 1997; Cahuzac and Poignant, 1997). The first occurrence of *Orbulina universa*, located near the top of the core 19R-1 (Fig. 9F, G), supports this hypothesis (Bolli et al., 1985).

The $^{87}Sr/^{87}Sr$ ratio obtained from the bivalve shell from the core 10R-2 yielded an estimated age of 8.40 Ma (late Tortonian; Fig. S1). No evidence of dissolution was observed through optical microscopy and SEM (Fig. 9I). Trace elements analysis indicates a composition similar to modern, pristine, aragonitic bivalves (Fig. S1; Ragland et al., 1979; Carrol and Romanek, 2008). Raman spectra, collected in different parts of the shell and compared with the reference spectra of carbonates provided in Borromeo et al. (2017), confirm an aragonitic composition, whereas calcite was never detected (Fig. S1).

4.4 Downhole logging data

Comparison of the downhole core log data (Emeis et al., 1996; Major et al., 1998) with the skeletal assemblage, facies distribution and petrographic characteristics (Fig. 5), highlights two major boundaries within Unit III (Fig. 10). The first, as recognised by Major et al. (1998), is located between the core 20R-1 and the core 19R-3 (Fig. 10). This corresponds to variations in the natural gamma ray intensity, mainly as a consequence of changes in the concentration of uranium and of the physical properties (the limestone becomes more porous and less homogeneous upcore; Fig. 10). This boundary also corresponds with the last occurrence of *Lepidocyclina* and *Miogypsina*, is also close to the first occurrence of *O. universa*, and to an increase in abundance of coralline algae (Fig. 5). The second major boundary is between the cores 15R-1 and 14R-1 (Fig. 10). The base of this boundary is marked by a decrease in porosity and, consequently, an increase in resistivity and in sonic velocity (Fig. 10). An increase in uranium concentration and gamma ray emissions marks the upper contact. This boundary corresponds to a layer of extensive recrystallization and an

important facies change (Fig. 5). The interval below this surface is dominated by coralline algae, whereas the one above is dominated by corals (Fig. 5). Minor changes in the downhole logs occur between the cores 11R-1 and 10R-2, and also between the cores 9R-1 and 8R-1 (Fig. 10). The former corresponds to the position of well-cemented layers of the core 10R-2, while the latter to the increase in micrite occurring between the cores 9R-1 and 8R-1.

5. Discussion

5.1 Stratigraphy

By integrating the various biostratigraphic and geochemical evidence, it is possible to refine the age assignment of the Miocene carbonates. Based on LBF, core 23R is Burdigalian (Cahuzac and Poignant, 1997; Özcan and Less, 2009; Özcan et al., 2009; BouDagher-Fadel and Price, 2010, 2013). The same assemblage characterises most of the LBF and echinoid facies (25R to 20R), and can be attributed to the same age. Only fragments of unidentifiable lepidocyclinids (without miogypsinids) were observed in core 26R; therefore the base of the succession can be either Burdigalian or slightly older.

The interval located between the recrystallized layer and the base of Unit II (14R-1 to 7R1; Fig. 5) is likely to be late Miocene, as indicated by the Sr isotope analyses of the pristine bivalve in core 10R-2 (Fig. S1). This is in agreement with the Sr isotope analysis performed on carbonates from Hole 965A (Major et al., 1998; Robertson, 1998b) and is supported by both LBF and plankton stratigraphy that indicate a middle to late Miocene age from core 20R upwards (Bolli et al., 1985; Betzler and Schmitz, 1997; Cahuzac and Poignant, 1997). The presence of deposits related to the Messian Salinity Crisis (Unit II) just above this interval is also consistent with a late Miocene age (Figs 3, 5; Major et al., 1998).

The interval between cores 19R-3 and 15R-1 is either of middle or late Miocene age, as suggested by both LBF and plankton stratigraphy. The observed *Heterostegina* is close to *H. papyracea* and *H. gomez-angulensis*. Both species are reported from the Tortonian (Papazzoni and

Sirotti, 1999; Tosquella et al. 2001; Daya and Bignot 2003). This would suggest a late Miocene age. However, the taxonomy of Neogene flat heterosteginds (sensu lato) is rather problematic, firstly due to the presence of different lineages that are recognized by some but not all authors (e.g. Freudenthal, 1969), and, secondly due to problems with the generic placement of some lineages (Papp and Küpper, 1954; Banner and Hodgkinson 1991; BouDagher-Fadel and Price 2014). Furthermore, species identification is strongly based on the size of the protoconch and on the number of undivided chambers following the embryo. Both parameters have been shown to be strongly influenced by environmental factors (Eder et al., 2017). Since facies rich in flat heterosteginds (sensu lato) occur also in the middle Miocene (e.g. Reuter and Piller, 2011), the sole presence of this species is not enough to support a late Miocene age. A late Miocene age for the interval between cores 19R-3 and 15R-1 would imply that the whole middle Miocene is missing from the Eratosthenes succession. This might have been caused by a prolonged period of low sedimentation-rate or by major erosion. A 5 million years long period of low sedimentation would be expected to have resulted in the formation of authigenic minerals (as observed during the hiatus between Eocene chalk and Miocene shallow-water carbonates), but such authigenic minerals are absent from core 20R and upcore. Also there is no clear evidence of major erosion, either sub-aerial or submarine. However, since the recovery of Hole 966F was poor, it is impossible to rule out either a hiatus in sedimentation or an erosional event. Based on the available data, the most likely age model seems to be lower Miocene from the base of Unit III up to core 20R, middle Miocene from cores 19R-3 to 15R-1, and late Miocene from the cores 14R-1 to the top of Unit III. Following this model, the boundary highlighted in downhole core log data between cores 20R and 19R-3 (Fig. 10; Emeis et al., 1996; Major et al., 1998), could correspond to the unconformity reported at the base of the middle Miocene in the basins surrounding the Eratosthenes Seamount (Hsü et al. 1978; Steinberg et al. 2011; Klimke and Ehrhardt, 2014).

5.2 Palaeoenvironmental reconstruction

LBF and hermatypic corals commonly occur in the succession, suggesting tropical conditions (Fig. 5; Betzler et al., 1997; Lees and Buller, 1972; Beavington-Penney and Racey, 2004). The results of SEDEX analysis indicate very low concentrations of biovailable-P throughout the whole Unit III (Fig. 8). These values are always below the boundary between non-oligotrophic and oligotrophic environments as proposed by Coletti et al. (2017) based on the study of Miocene carbonate systems in Italy and France. This evidence points toward oligotrophic conditions during the deposition of the Miocene shallow-water carbonates. Consistent with this hypothesis, heterotroph suspension-feeders that commonly thrive in nutrient-rich environments (Hallock and Schlager, 1986; Hallock, 1988; Brasier, 1995a, b; Halfar et al., 2004; Lokier et al. 2009; Reijmer et al., 2012; Reymond et al., 2016; Coletti et al., 2015, 2017), are almost absent (Table 1; Fig. 5). Oligotrophic conditions during the Miocene in the Eratosthenes Seamount area are also in agreement with modern evidence. The lowest average concentrations of chlorophyll α in the Mediterranean are recorded off-shore Cyprus (Barale and Zin, 2000; Basso et al., 2004). In the LBF and echinoid facies bioavailable-P values are higher than in the rest of Unit III (Fig. 8). Glaucony is common and highly evolved at the base of this facies, occurring as extremely large grains (Fig 6A, B). Upwards, glaucony is less common and the grains are smaller but the mineral is still remarkably evolved (Fig. 6D). Generally, the longer the grains stay at the water-sediment interface the more they increase in size and become greener due to uptake of iron and potassium (Odin and Matter, 1981). Since highly evolved glaucony grains cannot be produced unless the sedimentation rate is extremely low for a prolonged period of time (Odin and Matter, 1981), their presence is not consistent with active carbonate production from LBF and echinoids. A probable solution to this problem is that the glaucony grains were reworked from the surface that separates the Eocene chalk from the Miocene shallow-water carbonates. This surface accounts for an extremely long period of non-deposition, compatible with colour and size of the glaucony grains of the core 26R-1 (Fig. 6A,

B). During this period, the crests of the Eratosthenes Seamount remained in a relatively deep-water environment (as suggested by the planktonic foraminifera trapped within the glaucony grains; Fig. 6B) and was characterised by extremely low sedimentation rate. During the early Miocene, the crest was uplifted into photic-zone depth. In this shallow environment, exposed to currents, the highly evolved glaucony grains were reworked and mixed with the newly produced skeletal carbonate grains. Upwards, reworked glaucony grains become less common as the source of glaucony near the crest of the Eratosthenes Seamount was progressively covered by shallow-water carbonates. Since low sedimentation rates favour the formation of both authigenic glaucony and phosphates (Föllmi, 2016), authigenic phosphates, formed during the Eocene-Miocene hiatus, might also have been reworked in the LBF and echinoid facies, causing the higher concentrations of bioavailable-P.

Variations of water depth and environmental conditions at the crest of the Eratosthenes Seamount are recorded by the different facies. The benthic foraminiferal assemblage of the LBF and echinoid facies (26R-1 to 20R-1) is dominated by *Miogypsina*, *Lepidocyclina* and *Amphistegina*. Except for the lepidocyclinds of the core 26R-1, all the other observed LBF have thick tests (Fig. 5C, D, E) that are typical of shallow-water dwellers (Hallock et al., 1986; Hallock and Glenn, 1986; Beavington-Penney and Racey, 2004). In particular, *Amphistegina* T/D ratio suggests very shallow-water conditions (10-25 m; Mateu-Vicens et al. 2009). However, the T/D ratio should be interpreted cautiously (Eder et al., 2018). The presence of common planktonic foraminifera (especially at the base of the facies; Fig. 5) together with the lack of miliolids and other typical shallow-water dwellers suggest intermediate water depths (e.g. Hallock and Glenn, 1986; Beavington-Penney and Racey, 2004). Therefore, a middle shelf setting is proposed for this facies, ranging from 40-60 m near the base (cores 26R and 25R; Fig. 11) to 30-40 m near the top (cores 24R to 20R; Fig. 11).

The presence of hermatypic corals in the overlying rhodolith and coral facies (19R-3) points

to shallower-water conditions. The benthic foraminifera assemblage, with common thick specimens of *Amphistegina* and rare *Heterostegina*, also suggests relatively shallow conditions (Hallock and Glenn, 1986; Hohenegger et al., 2000; Beavington-Penney and Racey, 2004; Mateu-Vicens et al. 2009; Renema, 2018). The coralline algal assemblage, with Corallinales, Sporolithales and Hapalidiales, point to intermediate water depths (20-80 m; Adey and Macintyre, 1973; Adey, 1979, 1986; Adey et al., 1982; Minnerey et al., 1985; Perrin et al., 1995; Basso et al., 2009). Consequently a shallow middle shelf setting is proposed for this facies (20-30 m; Fig. 11).

The coralline algal and *Heterostegina* facies (19R-2 to 16R-2) is rich in epiphytic foraminifera (e.g. *Neoconorbina*, Fig. 6F, G) and coralline algal hooked crusts. Their presence correlates this facies to a seagrass/seaweeds meadow (Fig. 7D; Brasier, 1975; Beavington-Penney et al., 2004; Murray, 2006; Sola et al., 2013; Tomassetti et al., 2016). The occurrence of planktonic foraminifera and the generally fine-grained size are probably related to the baffling effect of the meadow (Fig. 5; Scoffin, 1970; Brasier, 1975; Gacia and Duarte, 2001). *Heterostegina* (Fig. 9D, E) specimens are very thin and flat, especially at the base of the facies (Fig. 5). In the modern environment, large and flat nummulitids with partitioned chambers are common in deep water since they are well adapted to dim light (Hohenegger, 2000; Hohenegger et al., 2000; Renema, 2006, 2018). Hapalidales, which generally dominate in dim-light conditions, are also present close to the base of the interval; upwards, shallow-water Corallinales are more common (Adey and Macintyre, 1973; Adey, 1979, 1986; Adey et al., 1982; Minnerey et al., 1985; Perrin et al., 1995). The dominance of deep photic zone dwellers does not necessarily implies deep-water since the meadow itself (or any such structured habitat) can provide a shaded seafloor (James and Bone, 2011; Eder et al., 2018). Furthermore, the baffling effect of the meadow provides sheltering from hydrodynamic energy, thus favoring flat and thin LBF (Eder et al., 2018). Nowadays, macroalgae can develop down to 70 m of water depth on isolated Mediterranean seamounts (Bo et al., 2011). Worldwide, seagrass and seaweed meadows are known to occur down to 40-60 m of water-depth, although deeper occurrences can not be ruled out (Duarte 1991; Graham et al. 2007). On these bases, a

middle shelf setting is proposed for this interval (cores 19R-2 to 16R-2), deeper close to the base (40-60 m; 19R-2 to 19R-1; Fig. 11) and shallower toward the top (30-40 m; 18R-2 to 16R-2; Fig. 11). The presence of coralline-algal bioconstructions is consistent with this interpretation since small coralligenous build-ups are often associated with seagrass meadows, both in modern environments and in the fossil record (e.g. Bracchi et al., 2016, 2017).

In the overlying rhodolith and coral facies (16R-1 to 15R-1) rhodoliths have a rather compact internal structure (Fig. 7E), suggesting at least moderate hydrodynamic energy (Basso 1998). The coralline algal assemblage, with common Corallinales and Sporolithales, points to intermediate water-depth (20-80 m; Adey and Macintyre, 1973; Adey, 1979, 1986; Adey et al., 1982; Minnerey et al., 1985; Perrin et al., 1995). Hermatypic corals suggest a shallow-water setting. A shallow middle shelf setting is proposed also for this facies (20-30 m; Fig. 11).

The coral-reef facies (14R-1 to 11R) is characterised by hermatypic corals with abundant miliolids (including common *B. melo melo* and *Dendritina*) and a coralline algal association dominated by Corallinales (Table 1; Fig. 5). This assemblage is clearly related to a shallow-water reef environment that was located in the inner part of the shelf (10-20 m; Fig. 11; Betzler and Schmitz, 1997; Perrin et al., 1995; Pomar, 2001; Murray, 2006; Civitelli and Brandano, 2005; Benisek et al., 2009). The presence of some Sporolithales is consistent with a shallow-water setting due to their broad bathymetric range, with shallow-water taxa recorded in both modern and fossil environments (Fravega et al., 1989; Minnery et al., 1985; Adey, 1986; Perrin et al., 1995; Basso et al., 2009; Coletti et al., 2018a).

The mollusc and benthic foraminifer facies (10R-2 to 7R-1) includes more molluscs, more small miliolids and less coral than the coral-reef facies (Table 1; Fig. 5), suggesting a transition toward a lagoonal environment (water depth < 10 m; Fig. 11; Hallock and Glenn, 1986; Beavington-Penney and Racey, 2004). The uppermost part of this interval, with abundant micrite, small miliolids and relatively common ostracods, represents a very shallow-water, low-energy, setting (Figs 5, 6Q, 11; Hallock and Glenn, 1986).

The mollusc and ostracod facies of the top of 7R-1 (Fig 5) probably represents a brackish environment (Fig. 11). This peculiar setting is consistent with the high concentrations of bioavailable-P of this facies (Fig. 8). Brackish facies are indeed recorded in the latest Messinian palaeotopography of the area, as documented from Cyprus onshore, the Cyprus slope and the Eratosthenes Seamount slope (Robertson, 1998c; Spezzaferri et al., 1998; Rouchy et al., 2001). Therefore, it is possible that brackish conditions briefly developed also on the top of the Eratosthenes Seamount during the beginning of Messinian Salinity Crisis.

5.3 Regional implications

Sedimentation at active margins is typically very complicated and detailed study and comparison are necessary to separate the effects of tectonic and global sea-level changes. Since the Miocene successions of the Eratosthenes Seamount and the one onshore Cyprus developed on different plates, their comparison can help in separating tectonic and global effects.

Cyprus was characterised by pelagic sedimentation during the Paleogene (Robertson 1976; Robertson et al., 1991). During the Oligocene – early Miocene a first localized phase of reef development occurred, known as the Terra Member of the Pakhna Formation (Robertson et al., 1991; Follows, 1992; Follows et al. 1996; Banner et al., 1999; BouDagher-Fadel and Lord, 2006). The Terra Member is characterised by hermatypic corals and a diverse LBF assemblage (Follows, 1992; Follows et al. 1996). These shallow-water carbonates drowned at the end of the early Miocene and were covered by hemipelagic marls (Robertson et al., 1991; Follows, 1992; Eaton and Robertson, 1993; Follows et al., 1996). During the Tortonian, a second and more widespread phase of shallow-water deposition occurred, known as the Koronia Member of the Pakhna Formation (Robertson et al. 1991; Eaton and Robertson, 1993; Follows, 1992; Follows et al. 1996). The Koronia Member is dominated by hermatypic corals that formed fringing reefs around the Troodos Massif; these reefs persisted until the Messian Salinity Crisis (Robertson et al., 1991; Follows, 1992; Eaton and Robertson, 1993; Follows et al., 1996).

In both the Eratosthenes Seamount and onshore Cyprus successions there is a change from pelagic to shallow-water deposition at the beginning of the Neogene. This is related to tectonic uplift, estimated as several hundred meters. This event can be generally attributed to the regional collision of the Eurasian (Anatolian) and African plates that caused compression and uplift of the overriding plate, as documented from southern Cyprus (Robertson et al., 1991; Eaton and Robertson 1993; Robertson, 1998 f; Kinnaird and Robertson, 2013) and uplift of the downgoing plate, probably via peripheral bulge uplift (Forsyth, 1980; Jacobi, 1981). The late Miocene is characterised by a further pulse of tectonic activity in Cyprus, especially in the north and west, which may be in part related to supra-subduction zone ('back arc') extension (Kinnaird and Robertson, 2013). Following the early Neogene uplift, the variations of water depth on the Eratosthenes Seamount are relatively small (Fig. 11). The brief deepening of the middle Miocene interval (Fig. 11), may be tentatively related to the early Langhian highstand (Haq et al., 1987; Miller et al., 2005). The late Miocene shallowing (Fig. 11) may be related to intensification of the inferred peripheral bulge, prior to collision with the subduction trench during Messinian to early Pliocene time, to global sea-level change or a combination of both. At the end of the Messinian both successions record the sea-level drop related to the Salinity Crisis.

From the perspective of environmental evolution, the Eratosthenes Seamount records three major biological events that characterised the Mediterranean basin as a whole: the reduction of diversity of LBF at the end of the early Miocene, the middle to late Miocene increase in coralline-algal abundance, and the latest Miocene expansion of coral reefs (Pomar et al., 2017).

At the end of the early Miocene, miogypsinids and lepidocyclinids rapidly declined in the Mediterranean. In contrast, both groups thrived for longer in the Indo-Pacific Ocean (Pomar et al., 2017; BouDagher-Fadel, 2018). Their decline on the Eratosthenes Seamount is remarkable in view of its proximity to the connection with the Indo-Pacific Ocean. After the end of the Burdigalian the diverse lower Miocene stock of the LBF and echinoid facies was replaced by an almost monospecific assemblage dominated by *Heterostegina* (Fig. 5). Since the temperature range of

Heterostegina is similar to those of *Baculogypsina* and *Baculogypsinoides* - considered the modern counterpart of the extinct lepidocyclinids and miogypsinids (Langer and Hottinger, 2000; Beavington-Penney and Racey, 2004; BouDagher-Fadel, 2018) - the decline of lower Miocene LBF was probably driven by oceanographic changes rather than decreases in yearly average temperatures. The cause was most likely the closure of the oceanic strand connecting the Mediterranean with the Indo-Pacific, which occurred in the early Miocene (Aktaş and Robertson, 1984; Ylmaz, 1993; Robertson, 1998e; Rögl, 1999). Major changes in the Mediterranean at the end of the early Miocene are also indicated by the beginning of sapropels deposition (Taylforth et al., 2014) and by the distribution of mollusc fauna (Piccoli et al., 1990).

The middle to late Miocene increase in coralline algal abundance is not restricted to the Mediterranean but is also recognised worldwide (Halfar and Mutti, 2005). This event has been related to an increased nutrient availability (Halfar and Mutti 2005; Pomar et al. 2017). In the Eratosthenes Seamount successions, coralline algae are especially common in the middle Miocene interval (Figs 5, 11), but an associated increase in bioavailable-P concentrations is not observed (Fig. 8).

The late Tortonian coral-reef expansion (Pomar, 1991; Buchbinder, 1996b; Esteban, 1996; Pedley, 1996; Vennin et al., 2004; Pomar and Hallock, 2007; Pomar et al., 2017) has been related to the coevolution of corals and zooxanthellae and to the late Miocene cooling (Pomar and Hallock, 2007; Pomar et al., 2017). These two events allowed corals to colonize shallow-water environments that, until that moment, were too warm and too bright for them (Pomar and Hallock, 2007; Pomar et al., 2017). Another hypothesis relates coral-reef expansion to the narrowing of the marine gateways with the Atlantic, that reduced the entry of cold oceanic waters, thus favouring local warming and increased salinity (Esteban, 1979; Pomar et al., 2017). Hermatypic corals occur both in the middle and upper Miocene intervals of the Eratosthenes Seamount, but they are really abundant only in the upper one, especially so in the coral-reef facies (Figs 5, 11). In the central interval, the corals are mainly associated with rotaliids and both deep-water and shallow-water coralline algae. In contrast,

in the uppermost interval, similarly to modern reef, they occur together with shallow-water miliolids and a coralline-algal assemblage that is largely dominated by shallow-water groups (Fig. 5). This is consistent with the hypothesis that corals colonized really shallow-water environment only during the late Miocene (Pomar and Hallock, 2007), but with this evidence alone is impossible to rule out alternative solutions.

6. Conclusions

The Miocene carbonates of the Eratosthenes Seamount formed in an oligotrophic tropical environment. Within the succession, it is possible to recognise three major intervals, characterised by different skeletal assemblages. The lower interval, of early Miocene age, is characterised by a large benthic foraminifera and echinoid skeletal assemblage that developed over deep-water Paleogene chalk uplifted to a water depth of 30-60 m. The central interval, of probable middle Miocene age, is dominated by coralline algae and corals in its basal part (20-30 m). Upwards, epiphytic foraminifera, hooked coralline-algal crusts and thin and flat specimens of *Heterostegina* dominate the core. This assemblage probably represents a seagrass/seaweed meadow (30-60 m). The uppermost part of the central interval is again dominated by coralline algae and corals (20-30 m). The uppermost interval is of late Miocene age. Its base recalls a typical modern reef assemblage with abundant corals, coralline algae and miliolids, compatible with a shallow water depositional environment (10-20 m). A lagoonal facies with small miliolids and molluscs characterises the top of the interval indicating further shallowing (less than 10 m). The shallow-water marine carbonates are overlain by ostracod-dominated brackish limestone and a limestone breccia, both related to the Messinian Salinity Crisis. These variations in water-depth during the Miocene were probably mainly controlled by the collision of the Eurasian and African plates. A similar situation also occurs

onshore Cyprus, indicating tectonic activity as the main driving force of sedimentation in the region.

On the general level, the Eratosthenes Seamount succession presents a lower Miocene with diverse and abundant large benthic foraminifera, an uppermost Miocene with coral-reefs and coralline-algal dominance in between. This trend is widespread among Miocene Mediterranean shallow-water carbonates and is most likely related to the general environmental evolution of the basin since its recorded also on an isolated platform, far away from terrestrial influx, like the Eratosthenes Seamount. The decline of miogypsinids and lepidocyclinids, which occurred on the Eratosthenes Seamount after the Burdigalian, is remarkable in view of its proximity to the gateway with the Indo-Pacific Ocean, where both groups thrived even in the middle Miocene. The early Miocene closure of the oceanic strand that connected the Mediterranean with the Indo-Pacific was probably the main cause of the decline of these large benthic foraminifera in the Mediterranean.

Acknowledgements

The authors are grateful to the International Ocean Drilling Program for providing the samples used in this study. We thank Holger Kulmann for his assistance with sampling at the Bremen Core Repository. Antonino Briguglio, Yossi Mart and a third anonymous reviewer provided helpful comment on the originally submitted manuscrip. Special thank also goes to Christoph Neururer, Stephanie Stainbank and Valentina Beccari for their assistance during CT-Scanning. Elisa Malinverno kindly provided funding for the Sr isotope analyses, Dieter Buhl performed the analyses in Bochum, John McArthur licensed to use the LOWESS 5, and Mariano Parente provided useful advices on Sr stratigraphy. We also thank Sergio Andò, Eduardo Garzanti and Giovanni Vezzoli (Laboratory for Provenance Studies of Milano-Bicocca University) for their help with Raman analyses and their useful suggestions. The first author participated to the Edimburg University Field Trip in Cyprus and would like to thank Dick Kroon, Elizabeth Balmer, Louis Kinnear, Geoff Bromiley, Gillian McCay and Yili Yang, for their clarification on Cyprus

geology. AM would like to thank the Israeli Ministry of Energy and the Maurice Hatter Foundation for their support for his travels and his research activity. This is a scientific contribution of Project MIUR - Dipartimenti di Eccellenza 2018-2022.

References

Adams, C.G., Benson, R.H., Kidd, R.B., Ryan, W.B.F., Wright, R.C., 1977. The Messinian salinity crisis and evidence of late Miocene eustatic changes in the world ocean. Nature. 269, 383-386.

Adey, W.H., 1979. Crustose coralline algae as microenvironmental indicators in the Tertiary, in: Gray, J., Boucot, A.J. (Eds.), Historical Biogeography, Plate Tectonics and the changing environment. Proceedings of the thirty-seventh Annual Biology Colloquium, pp. 459-464.

Adey, W.H., 1986. Coralline algae as indicators of sea-level, in: Van de Plassche, O. (Ed.), Sea-level research: a manual for the collection and evaluation of data. Geo-Books, Norwich, pp. 229-280.

Adey, W.H., Macintyre, I.G., 1973. Crustose coralline algae: a re-evaluation in the geological sciences. Geological Society of America Bulletin. 84, 883-904.

Adey, W.H., Townsend, R.A., Boykins, W.T., 1982. The crustose coralline algae (Rhodophyta: Corallinaceae) of the Hawaiian Islands. Smithsonian contribution to Marine Sciences 15.

Aktaş, G., Robertson, A.H.F., 1984. The Maden Complex, SE Turkey: evolution of a Neotethyan active margin, in: Dixon, J.E., Robertson, A.H.F. (Eds.), The Geological evolution of the Eastern

Mediterranean. Geological Society Special Publication 17, Geological Society, London, pp. 375-402.

Amato, V., Drooger, C.W., 1969. How to measure the angle γ in the Miogypsinidae. Revista Española de Micropaleontologia. 1, 19-24.

Amorosi, A., 1995. Glaucony and sequence stratigraphy: a conceptual framework of distribution in siliciclastic sequences. Journal of Sedimentary Research. 65, 419-425.

Amorosi, A., 1997. Detecting compositional, spatial, and temporal attributes of glaucony: a tool for provenance research. Sedimentary Geology. 109, 135-153.

Banner, F.T., Hodginkson, R.L., 1991. A revision of the foraminiferal subfamily heterostegininae. Revista Espaňola de Micropaleontologia. 23, 101-140.

Banner F.T., Lord A.R., BouDagher-Fadel M.K. (1999) – The Terra Limestone Member (Miocene) of western Cyprus. Greiswalder Geowissenschaftliche Beiträge, 6, 489-501.

Barale, V., Zin, I., 2000. Impact of continental margins in the Mediterranean Sea: Hints from the surface colour and temperature historical record. Journal of Coastal Conservation. 6, 5-14.

Basso, D., 1998, Deep rhodolith distribution in the Pontian Islands, Italy: a model for the paleoecology of a temperate sea. Palaeogeography Palaeoclimatology Palaeoecology. 137, 173-187.

Basso, D., Thompson, J., Corselli, C., 2004. Indications of low macrobenthic activity in the deep sediments of the eastern Mediterranean Sea. Scientia Marina. 68 (suppl. 3), 53-62.

Basso, D., Nalin, R., Nelson, C.S., 2009. Shallow-water *Sporolithon* rhodoliths from North Island (New Zealand). Palaios. 24, 92-103.

Beavington-Penney, S.J., Racey, A., 2004. Ecology of extant nummulitids and other large benthic foraminifera in paleoenvironmental analysis. Earth Sciences Reviews. 67, 219-265.

Beavington-Penney, S.J., Wrigth, V.P., Woelkerling, W.J., 2004. Recognising macrophyte-vegetated environments in the rock record: a new criterion using 'hooked' forms of crustose coralline red algae. Sedimentary Geology. 166, 1-9.

Betzler, C., Schmitz, S., 1997. First record of *Borelis Melo* and *Dendritina* sp. in the Messinian of SE Spain (Capo de Gata, Province Almeria). Palaöntologische Zeitschrift. 71, 211-216.

Betzler, C., Brachert, T.C., Nebelsick, J., 1997. The warm temperate carbonate province: a review of the facies, zonations and delimitations. Courier Forschungsinstitut Senkenberg. 201, 83–99.

Ben-Avraham, Z., Ginzburg, A., Makris, J., Eppelbaum, L., 2002. Crustal structure of the Levant Basin, eastern Mediterranean. Tectonophysics. 346, 23-43.

Benedetti, A., Less, G., Parente, M., Pignatti, J., Cahuzac, B., Torres-Silva, A.I., Buhl, D., 2017. *Heterostegina matteuccii* sp. nov. (Foraminiferida: Nummulitidae) from the lower Oligocene of Sicily and Aquitaine: a possible transatlantic immigrant. Journal of Systematic Palaeontology. http://dx.doi.org/10.1080/14772019.2016.1272009

Benisek, M.F., Betzler, C., Marcano, G., Mutti, M., 2009. Coralline-algal assemblages of a Burdigalian platform slope: implications for carbonate platform reconstruction (northern Sardinia, western Mediterranean Sea). Facies. 55, 375-386.

Bo, M., Bertolino, M., Borghini, M., Castellano, M., Harriague, A.C., DiCamillo, C.G., Gasparini, G., Misic, C., Povero, P., Pusceddu, A., Schroeder, K., Bavestrello, G., 2011. Characteristics of the Mesophotic Megabenthic Assemblages of the Vercelli Seamount (North Tyrrhenian Sea). Plos One. 6, e16357, doi:10.1371/journal.pone.0016357

Bolli, H.M., Saunders, J.B., Perch-Nielsen, K., 1985. Plankton stratigraphy Vol. 1. Cambridge University Press, Cambridge.

BouDagher-Fadel, M. K., Lord, A., 2006. Illusory stratigraphy decoded by Oligocene-Miocene autochthonus foraminifera in the Terra Member, Pakhna Formation (Cyprus). Stratigraphy. 1, 217-226.

BouDagher-Fadel, M. K., Price, G.D., 2010. Evolution and paleogeographic distribution of the lepidocyclinids. Journal of Foraminiferal Research. 40, 79-108.

BouDagher-Fadel, M.K., Price, G.D., 2013. The phylogenetic and palaeogeographic evolution of the miogypsinid larger benthic foraminifera. Journal of the Geological Society of London. 170, 185-208.

BouDagher-Fadel, M.K., Price, G.D., 2014. The phylogenetic and palaeogeographic evolution of the nummulitoid larger benthic foraminifera. Micropaleontology. 60, 483-508.

BouDagher-Fadel, M.K., 2018. Evolution and geological significance of larger benthic foraminifera. University College London Press, London.

Borromeo, L., Zimmerman, U., Andò, S., Coletti, G., Bersani, D., Basso, D., Gentile, P., Schulz, B., Garzanti, E., 2017. Raman spectroscopy as a tool for magnesium estimation in Mg-calcite. Journal of Raman Spectroscopy. 48, 983-992.

Bracchi, V.A., Nalin, R., Basso, D., 2016. Morpho-structural heterogeneity of shallow-water coralligenous in a Pleistocene marine terrace (Le Castella, Italy). Palaeogeography Palaeoclimatology Palaeoecology. 454, 101-112.

Bracchi, V.A., Savini, A., Basso, D., Marchese, F., Corselli, C., 2017. Coralligenous morphotypes on subhorizontal substrate: a new categorization. Continental Shelf Research. 144, 10-20.

Braga, J.C., Bosence, D.W.J., Steneck, R.S., 1993. New anatomical characters in fossil coralline algae and their taxonomic implications. Paleontolog., 36, 535-547.

Brasier, M.D., 1975. An outline history of seagrass communities. Palaeontology. 18, 681-702.

Brasier, M.D., 1995A. Fossil indicators of nutrient levels 1: eutrophication and climate change, in: Bosence, D.W.J., Allison, P.A. (Eds.), Marine Paleoenvironmental Analysis from Fossils. Geological Society Special Publication 83. pp. 113–132.

Brasier, M.D., 1995B. Fossil indicators of nutrient levels 2: evolution and extinction in relation to oligotrophy, in: Bosence, D.W.J., Allison, P.A. (Eds.), Marine Paleoenvironmental Analysis from Fossils. Geological Society Special Publication 83. pp. 133–150.

Briguglio, A., Hohenegger, J., Less, G., 2013. Paleobiological applications of three-dimensional biometry on larger benthic foraminifera: A new route of discoveries. Journal of Foraminiferal Research. 43, 67-82.

Briguglio, A., Wöger, J., Wolfgring, E., Hohenegger, J., 2014. Changing investigation perspectives: methods and applications of computed tomography on larger benthic foraminifera, in: Kitazato, H., Bernhard, J. (Eds.), Experimental Approaches in Foraminifera: Collection, Maintenance and Experiments. Environmental Science Series, Springer, Japan. pp. 55-70.

Briguglio, A., 2018. The Miocene (Burdigalian) lepidocyclinids and miogypsinids of Channa Kodi, Padappakkara, Kerala, Southern India. Palaeontographica, Abteilung A: Palaeozoology – Stratigraphy. 312, 1-15.

Buchbinder, B., 1996A. Miocene carbonates of the Eastern Mediterranean, the Red Sea and the Mesopotamian Basin: geodynamic and eustatic controls, in: Franseen, E.K., Esteban, M., Ward, W.C., Rouchy, J.M., (Eds.), Models for carbonate stratigraphy, from Miocene reef complex of the Mediterranean area. Concepts in Sedimentology and Paleontology 5, Society for Sedimentary Geology, Tulsa, Oklaoma, U.S.A. pp. 89-96.

Buchbinder, B., 1996B. Middle and upper Miocene reefs and carbonate platforms in Israel, in: Franseen, E.K., Esteban, M., Ward, W.C., Rouchy, J.M., (Eds.), Models for carbonate stratigraphy, from Miocene reef complex of the Mediterranean area. Concepts in Sedimentology and Paleontology 5, Society for Sedimentary Geology, Tulsa, Oklaoma, U.S.A. pp. 333-345.

Cahuzac, B., Poignant, A., 1997. Essai de biozonation de l'Oligo-Miocène dans le bassins européens à l'aide des grands foraminifères néritique. Bulletin de la Société géologique de France. 168, 155-169.

Carrol, M., Romanek, C.S., 2008. Shell layer variation in trace element concentration for the freshwater bivalve Elliptio complanata. Geo-Marine Letters. 28, 369-381.

Chaproniere, G.C.H., 1980. Biometrical studies of early Neogene larger Foraminiferida from Australia and New Zealand. Alcheringa. 4, 153-181.

Civitelli, G., Brandano, M., 2005. Atlante delle litofacies e modello deposizionale dei Calcari a Briozoi e Litotamni nella Piattaforma carbonatica laziale-abruzzese. Bollettino Società Geologica Italiana. 124, 611-643.

Coletti, G., Basso, D., Frixa, A., Corselli, C., 2015. Transported rhodoliths witness the lost carbonate factory: a case history from the Miocene Pietra da Cantoni limestone (NW Italy). Rivista Italiana di Paleontologia e Stratigrafia. 121, 345-368.

Coletti, G., El Kateb, A., Basso, D., Cavallo, A., Spezzaferri, S., 2017. Nutrient influence on fossil carbonate factories: Evidence from SEDEX extractions on Burdigalian limestones (Miocene, NW Italy and S France). Palaeogeography Palaeoclimatology Palaeoecology. 475, 80-92.

Coletti, G., Basso, D., Corselli, C., 2018A. Coralline algae as depth indicators in the Sommières Basin (early Miocene, Southern France). Geobios. 51, 15-30.

Coletti, G., Stainbank, S., Fabbrini, A., Spezzaferri, S., Foubert, A., Kroon, D., Betzler, C., 2018B. Biostratigraphy of large benthic foraminifera from Hole U1468A (Maldives): A CT-scan taxonomic approach. Swiss Journal of Geosciences. 111, 523-536.

Daya, D., Bignot, G., 2003. *Heterostegina papyracea* Seguenza from the Miocene South Rifian Corridor (Morocco): biometry and paleocological particularities. Geobios. 38, 187-196.

De Bock, F.J., 1973. Embryonal structures of *Miogypsina*. Scripta Geologica. 18, 1-15.

Dercourt, J., Gaetani, M., Vrielynk, B., Barrier, E., Biju-Duval, B., Brunet, M.F., Cadet, J.P, Crasquin, S., Sandulescu, M., 2000. Atlas Peri-Tethys, Palaeogeographical Maps.

Drooger, C.W., 1993. Radial Foraminifera; morphometrics and evolution. Verhandelingen der Koninklijke Nederlandse Akademie van Wetenschappen. Afdeling Natuurkunde. 41, 1–242.

Drooger, C.W., Socin, C., 1959. Miocene foraminifera from Rosignano, northern Italy. Micropaleontology. 5, 415–426.

Duarte, C.M., 1991. Sea grass depth limit. Aquatic Botany. 40, 363-377.

Eaton, S., Robertson, A.H.F., 1993. The Miocene Pakhna Formation, southern Cyprus and its relationship to the Neogene tectonic evolution of the Eastern Mediterranean. Sedimentary Geology. 86, 273-296.

Eder, W., Hohenegger, J., Briguglio, A., 2017. Depth-related morphoclines of megalospheric tests of Heterostegina depressa d'Orbigny: biostratigraphic and paleobiological implications. Palaios. 32, 110-117.

Eder, W., Hohenegger, J., Briguglio, A., 2018. Test flattening in the larger foraminifer Heterostegina depressa: predicting bathymetry from axial sections. Paleobiology. 44, 76-88.

Emeis, K.C., Robertson, A.H.F., Richter, C., et al., 1996. Proceedings of the Ocean Drilling Program, Initial Reports 160. Ocean Drilling Program, College Station, Texas, U.S.A.

Esteban, M., 1979. Significance of the upper Miocene coral reefs of the western Mediterranean. Palaeogeography Palaeoclimatology Palaeoecology. 29, 169-188.

Esteban, M., 1996. An overiew of of Miocene reefs from Mediterranean areas: general trends and facies models, in: Franseen, E.K., Esteban, M., Ward, W.C., Rouchy, J.M., (Eds.), Models for carbonate stratigraphy, from Miocene reef complex of the Mediterranean area. Concepts in Sedimentology and Paleontology 5, Society for Sedimentary Geology, Tulsa, Oklaoma, U.S.A. pp. 3-53.

Feld, C., Mechie, J., Hübscher, C., Hall, J., Nicolaides, S., Gurbuz, C., Bauer, K., Louden, K., Weber, M., 2017. Crustal structure of the Eratosthenes Seamount, Cyprus and S. Turkey from an amphibian wide-angle seismic profile. Tectonophysics. 700-701, 32-59.

Fravega, P., Piazza, M., Vannucci, G., 1989. *Archaeolithothamnium* Rothpletz, inidicatore ecologico-stratigrafico?. Simposio di Ecologia e Paleoecologia delle Comunità Bentoniche 1985 Atti. 3, 729-743.

Föllmi, K.B., 2016. Sedimentary condensation. Earth-Sciences Reviews. 152, 143–180.

Follows, E.J., 1992. Patterns of reef sedimentation and diagenesis in the Miocene of Cyprus. Sedimentary Geology. 79, 225-253.

Follows, E.J., Robertson, A.H.F., Scoffin, T.P., 1996. Tectonic control on Miocene reefs and related carbonate facies in Cyprus, in: Franseen, E.K., Esteban, M., Ward, W.C., Rouchy, J.M. (Eds.), Models for carbonate stratigraphy, from Miocene reef complex of the Mediterranean area. Concepts in Sedimentology and Paleontology 5, Society for Sedimentary Geology, Tulsa, Oklaoma, U.S.A. pp. 295-315.

Forsyth, D.W., 1980. Comparison of Mechanical Models of the Oceanic Lithosphere. Journal of Geophysical Research. 85, 6364-6468.

Flügel, E. 2010. Microfacies of Carbonate Rocks: Analysis Interpretation and Application. Springer, New York.

Gacia, E., Duarte, C.M., 2001. Sediment retention by a Mediterranean *Posidonia oceanica* meadow:

the balance between deposition and resuspension. Estuarine Coastal and Shelf Science. 52, 505-514.

Gardosh, M.A., Garfunkel, Z., Druckman, Y., Buchbinder, B., 2010. Tethyan rifting in the Levant Region and its role in Early Mesozoic crustal evolution, in: Homberg, C., Bachmann, M. (Eds.) - Evolution of the Levant Margin and Western Arabian Platfrom since the Mesozoic. Geological Society Special Publication 341, London. pp. 9-36.

Garfunkel, Z., 2004. Origin of the Eastern Mediterranean basin: a reevaluation. Tectonophysics. 298, 63-82.

Graham, M.H., Kinlan, B.P., Druehl, L.D., Garske, L.E., Banks, S., 2007. Deep-water kelp refugia as potential hotspots of tropical marine diversity and productivity. PNAS. 104, 16576 –16580.

Harvey, A.S., Broadwater, S.T., Woelkerling, W.J., Mitrovski, P.J., 2003. *Choreonema* (Corallinales, Rhodophyta): 18S rDNA phylogeny and resurrection of the Hapalidiaceae for the subfamilies Choreonematoideae, Austrolithoideae, and Melobesioideae. Journal of Phycology. 39, 988-998.

Hallock, P., 1988. The role of nutrient availability in bioerosion: consequences to carbonate buildups. Palaeogeography Palaeoclimatology Palaeoecology. 63, 275–291.

Hallock, P., Glenn, C., 1986. Larger Foraminifera: A Tool for Paleoenvironmental Analysis of Cenozoic Carbonate Depositional Facies. Palaios. 1, 55-64.

Hallock, P., Schlager, W., 1986. Nutrient excess and the demise of coral reefs and carbonate platforms. Palaios. 1, 389–398.

Hallock, P., Forward, L.B., Hans J.H., 1986. Influence of environment on the test shape of *Amphistegina*. Journal of Foraminiferal Research. 16, 224-231.

Halfar, J., Godinez-Orta, L., Mutti, M., Valdez-Holguìn, J.E., Borges, J.M., 2004. Nutrient and temperature controls on modern carbonate production: an example from the Gulf of California. Mexico. Geology. 32, 213–216.

Halfar, J., Mutti, M., 2005. Global dominance of coralline red-algal facies: A response to Miocene oceanographic events. Geology. 33, 481-484.

Haq, B.U., Hardenbol, J., Vail, P.R., 1987. Chronology of Fluctuating Sea Levels Since the Triassic. Science. 235, 1156-1166.

Hohenegger, J., 2000. Coenoclines of larger foraminifera. Micropaleontology. 46, 127-151.

Hohenegger, J., Yordanova, E., Hatta, A., 2000. Remarks on West Pacific Nummulitidae (Foraminifera). Journal of Foraminiferal Research. 30, 3-28.

Hohenegger, J., 2011. Growth-invariant Meristic Characters Tools to Reveal Phylogenetic Relationships in Nummulitidae (Foraminifera). Turkish Journal of Earth Sciences. 20, 655-681.

Hsü, K.J., Ryan, W.B.F., Cita, M.B., 1973. Late Miocene dessiccation of the Mediterranean. Nature. 242, 240- 244.

Hsü, K.J., Montadert, L., et al., 1978. Initial Report of the Deep Sea Drilling Project. DSPD 42 (Part 1). Washington (U.S. Govt. Printing Office), U.S.A.

Jacobi, R.D., 1981. Peripheral bulge a causal mechanism for the Lower/Middle Ordovician unconformity along the western margin of the Northern Appalachians. Earth and Planetary Science Letters. 56, 245-251.

James, N.P., Bone, Y., 2011. Carbonate production in a warm-temperate macroalgal environment, Investigator Strait, South Australia. Sedimentary Geology. 240, 41-53.

Kinnaird, T., Robertson, A.H.F., Morris, A., 2011. Timing of uplift of the Trodos Massif (Cyprus) constrained by sedimentary and magnetic polarity evidence. Journal of the Geological Society of London, 168, 457-470.

Kinnaird, T., Robertson, A.H.F., 2013. Tectonic and sedimentary response to subduction and incipient collision in southern Cyprus easternmost Mediterranean region, in: Robertson, A.H.F., Parlak, O., Ünlügenç, U.C. (Eds.), Geological development of Anatolia and the Easternmost Mediterranean Region. Geological Society, London, Special Publications 372. pp. 585-614.

Klimke, J., Ehrhardt, A., 2014. Impact and implications of the Afro-Eurasian collision south of Cyprus from reflection seismic data. Tectonophysics. 626, 105-119.

Lagabrielle, Y., Goddéris, Y., Donnadieu, Y., Malavieille, J., Suarez, M., 2009. The tectonic history of Drake Passage and its possible impacts on global climate. Earth and Planetary Sciences Letters. 279, 197–211.

Langer, M.R., Hottinger, L., 2000. Biogeography of selected ‘‘larger’’ foraminifera. Micropaleontology. 46, 105-126.

Larsen, H.C., Saunders, A.D., Clift, P.D., Wei, W., Spezzaferri, S.m ODP Leg 152 Scientific Party, 1994. Seven Million Years of Glaciation in Greenland. Science. 264, 952-955.

Lees, A., Buller, A.T., 1972. Modern temperate-water and warm-water shelf carbonate sediments contrasted. Marine Geology. 13, 67–73.

Le Gall, L., Payri, C., Bittner, L., Saunders, G.W., 2009. Multigene polygenetic analyses support recognition of the Sporolithales, ord. Nov. Molecular Phylogenesis and Evolution. 54, 302-305.

Lewis, A.R., Marchant, D.R., Ashworth, A.C., Hemming, S.R., Machlus, M.L., 2007. Major middle Miocene global climate change: evidence from East Antarctica and the Transantarctic Mountains. GSA Bullettin. 119, 1449-1461.

Lokier, S.W., Wilson, M.E.J., Burton, L.M., 2009. Marine biota response to clastic sediment influx: A quantitative approach. Palaeogeography Palaeoclimatology Palaeoecology. 281, 25-42.

Major, C.O., Ryan, W.B.F, Jurado-Rodríguez M.J., 1998. Evolution of Paleoenvironments of Eratosthenes Seamount based on downhole logging integrated with carbonate petrology and reflection profiles, in: Robertson, A.H.F., Emeis, K.C., Richter, C., Camerlenghi, A. (Eds.), Proceedings of the Ocean Drilling Program, Scientific Results 160. pp. 483-508.

Major, C., Ryan, W.B.F., 1999. Eratosthenes Seamount: Record of late Miocene sea-level changes and facies related to the Messinian salinity crisis. Memorie Società Geologica Italiana. 54, 47-59.

Marlow, L., 2014. Tectonostratigraphic History and Petroleum Potential of the Levantine Basin, Eastern Mediterranean, in: Marlow, L., Kendall, C., Yose, L. (Eds.), Petroleum systems of the Tethyan region. AAPG memoir 106. pp. 279-299.

Mart, Y., Robertson, A.H.F., 1998. Eratosthenes Seamount: an oceanographic yardstick recording the late Mesozoic-Tertiary geological history of the Eastern Mediterranean, in: Robertson, A.H.F., Emeis, K.C., Richter, C., Camerlenghi, A. (Eds.), Proceedings of the Ocean Drilling Program, Scientific Results 160. pp. 701-708.

Mart, Y., Ryan, W.B.F., 2002. The complex tectonic regime of the Cyprus Arc: A short review. Israelian Journal of Earth Sciences. 51, 117-134.

Mascle, J., Benkhelil, J., Bellaiche, G., Zitter, T., Woodside, J., Loncke, L. & The Prismed II Scientific Party, 2000. Marine geologic evidence for a Levantine-Sinai plate, a new piece of the Mediterranean puzzle. Geology. 28, 779-782.

Mateu-Vicens, G., Hallock, P., Brandano, M., 2009. Test shape variability of Amphistegina d'Orbigny 1826 as a paleobathymetric proxy: application to two Miocene examples, in: Demuchuck, T., Gary, A. (Eds.), Geologic problems solving with microfossils. SEPM special publication 93. pp. 67-82.

Matteucci, R., Schiavinotto, F., 1977. Studio biometrico di *Nephrolepidina*, *Eulepidina* e *Cycloclypeus* in due campioni dell'Oligocene di Monte La Rocca, L'Aquila (Italia centrale). Geologica Romana. 16, 141-171.

McArthur, J.M., Howarth, R.J., Shields, G.A., 2012. Strontium Isotope Stratigraphy, in Gradstein, F.M., Ogg, J.G., Schmitz, M., Ogg, G. (Eds.), The Geologic Time Scale 2012, Elsevier. pp. 127-144.

Meilijson, I.A., Ashckenazi-Polivoda, S., Ron-Yankovich, L., Illner, P., Alsenz, H., Speijer, R.P., Almogi-Labin, A., Feinstein, S., Berner, Z., Püttmann, W., Abramovich, S., 2014. Chronostratigraphy of the Upper Cretaceous high productivity sequence of the southern Tethys, Israel. Cretaceous Research. 50, 187-213.

Meilijson, A., Ashckenazi-Polivoda, S., Illner, P., Alsenz, H., Speijer, R.P., Almogi-Labin, A., Feinstein, S., Püttmann, W., Abramovich, S., 2015. Evidence for specific adaptations of fossil benthic foraminifera to anoxic–dysoxic environments. Paleobiology. 42, 77-97.

Minnery, G.A., Rezak, R., Bright, T.J., 1985. Depth zonation and growth form of crustose coralline algae: Flower Garden Banks, Northwestern Gulf of Mexico, in: Toomey, D.F., Nitecki, M.H. (Eds.), Paleoalgology: Contemporary Research and Applications. Springer, New York. pp. 237-246.

Miller, K.G., Kominz, M.A., Browning, J.V., Wright, J.D, Mountain, G.S., Katz, M.E., Sugarman, P.J., Cramer, B.S., Christie-Blick, N., Pekar, S.F., 2005. The Phanerozoic Record of Global Sea-Level Change. Science. 310, 1293-1298.

Montadert, L., Nicholaides, S., Semb, P.H., Lie, O., 2014. Petroleum systems offshore Cyprus, in: Marlow, L., Kendall, C., Yose, L. (Eds.), Petroleum systems of the Tethyan region. AAPG memoir 106. pp. 301-334.

Murray, J.W., 2006. Ecology and applications of benthic foraminifera. Cambrige University Press, Cambridge.

Nelson, W.A., Sutherland, J.E., Farr, T.J., Hart, D.R., Neill, K.F., Kim, H.J., Yoon, H.S., 2015. Multi-gene phylogenetic analyses of New Zealand coralline algae *Corallinapetra novaezelandiae* gen. et sp. nov. and recognition of the Hapalidiales ord. nov. Journal of Phycology. 51, 454-468.

Odin, G.S., Letolle, R., 1980. Glauconitization and Phosphatization Environments: a Tentative Comparison, in: Bentor, Y.K. (Ed.), Marine Phosphorites – Geochemistry, occurrences, genesis. SEPM Special Publications 29. pp. 227-237.

Odin, G.S., Matter, A., 1981. De Glauconiarum origine. Sedimentology. 28, 611-641.

Özcan, E., Less, G., 2009. First record of the co-occurrence of western tethyan and indo-pacific

larger foraminifera in the Burdigalian of the Mediterranean province. Journal of Foraminiferal Research. 39, 23-39.

Özcan, E., Less, G., Báldi-Beke, M., Kollányi, K. Acar, F., 2009. Oligo-Miocene foraminiferal record (Miogypsinidae, Lepidocyclinidae and Nummulitidae) from the Western Taurides (SW Turkey): Biometry and implications for the regional geology. Journal of Asian Earth Sciences. 34, 740–760.

Papadimitriou, N., Gorini, C., Nader, F.H., Deschamps, R., Symeou, V., Lecomte, J.C., 2018. Tectono-stratigraphic evolution of the western margin of the Levant Basin (offshore Cyprus). Marine and Petroleum Geology, doi:10.1016/j.marpetgeo.2018.02.006.

Papazzoni, C.A., Sirotti, A., 1999. *Heterostegina papyracea* Seguenza, 1880 from the upper Miocene of Cessaniti (Vibo Valentia, Calabria, southern Italy). Bollettino della Società Paleontologica Italiana. 38, 15-21.

Papp, A., Küpper, K., 1954. The genus *Heterostegina* in the upper Tertiary of Europe. Contribution from the Cushman foundation for foraminiferal research. 5, 108-127.

Peck, J.M., 2008. Giant oil prospects lie in distal portions of offshore East Mediterranean basin. Oil and Gas Journal. 106, 41-49.

Pedley, M., 1996. Miocene reef distributions and associations in the Central Mediterranean region: and overview, in: Franseen, E.K., Esteban, M., Ward, W.C., Rouchy, J.M. (Eds.), Models for carbonate stratigraphy, from Miocene reef complex of the Mediterranean area. Concepts in Sedimentology and Paleontology, 5, Society for Sedimentary Geology, Tulsa, Oklaoma, U.S.A. pp. 73-345.

Perrin, C., Bosence, D.W.J., Rosen, B., 1995. Quantitative approaches to palaeozonation and palaeobathymetry of corals and coralline algae in Cenozoic reefs, in: Bosence, D.W.J., Allison, P.A. (Eds.), Marine Palaeoenvironmental Analysis from Fossils. Geological Society Special Publication 83. pp. 181-229.

Perrin, C., Bosellini, F.R., 2012. Paleobiogeography of scleractinian reef corals: Changing patterns during the Oligocene–Miocene climatic transition in the Mediterranean. Earth Sciences Review. 111, 1-24.

Piccoli, G., Sartori, S., Franchino, A., 1990. Mathematical paleobiogeography (exemplified for the shallow Tethys in the Tertiary), in: Kotaka, T., Dickins, J.M., McKenzie, K.G., Mori, K., Ogasawara, K., Stanley, G.D.J. (Eds.), Shallow Thethys 3, Proceedings of the International Symposium on Shallow Tethys, Sendai, Japan. pp. 59-68

Pomar, L., 2001. Ecological control of sedimentary accommodation: evolution from a carbonate ramp to rimmed shelf, Upper Miocene, Balearic Islands. Palaeogeography Palaeoclimatology Palaeoecology. 175, 249-272.

Pomar, L., Hallock, P., 2007. Changes in coral-reef structure through the Miocene in the Mediterranean province: Adaptive versus environmental influence. Geology. 35, 899-902.

Pomar, L., Baceta, J.I., Hallock, P., Mateu-Vicens, G., Basso, D., 2017. Reef building and carbonate production modes in the west-central Tethys during the Cenozoic. Marine and Petroleum Geology. 83, 261-304.

Premoli-Silva, I., Spezzaferri, S., D'Angelantonio, A., 1998. Cretaceous foraminiferal bio-isotope stratigraphy of Hole 967E and Paleogene planktonic foraminiferal biostratigraphy of Hole 966F, Eastern Mediterranean, in: Robertson, A.H.F., Emeis, K.C., Richter, C., Camerlenghi, A. (Eds.), Proceedings of the Ocean Drilling Program, Scientific Results 160. pp. 377-394.

Ragland, P.C., Pilkey, O.H., Blackwelder, B.W., 1979. Diagenetic changes in the elemental composition of unrecrystallized mollusk shells. Chemical Geology. 25, 123-134.

Reijmer, J.J.G., Bauch, T., Schäfer, P., 2012. Carbonate facies patterns in surface sediments of upwelling and non-upwelling shelf environments (Panama, East Pacific). Sedimentology. 59, 32-56.

Renema, W., 2006. Large benthic foraminifera from the deep photic zone of a mixed siliciclastic-carbonate shel off East Kalimantan, Indonesia. Marine Micropaleontology. 58, 73-82.

Renema, W. 2018. Terrestrial influence as a key driver of spatial variability in large benthic

foraminiferal assemblage composition in the Central Indo-Pacific. Earth Sciences Review. 177, 514-544.

Reuter, M., Piller, W.E., 2011. Volcaniclastic events in coral-reef and seagrass environments: evidence for disturbance and recovery (Middle Miocene, Styrian Basin, Austria). Coral Reefs. 30, 889-899.

Reymond, C.E., Zihrul, K.S., Halfar, J., Riegl, B., Humphreys, A., Hildegard, W., 2016. Heterozoan carbonates from the equatorial rocky reefs of the Galapagos Archipelago. Sedimentology. 63, 940-958.

Robertson, A.H.F., 1976. Pelagic chalks and calciturbidites from the lower Tertiary of the Troodos Massif, Cyprus. Journal of Sedimentary Petrology. 46, 1007-1016.

Robertson, A.H.F., 1998A. Lithofacies evidence for the Cretaceous-Paleogene sedimentary history of Eratosthenes Seamount, Eastern Mediterranean, in its regional tectonic context (Sites 966 and 967), in: Robertson, A.H.F., Emeis, K.C., Richter, C., Camerlenghi, A. (Eds.), Proceedings of the Ocean Drilling Program, Scientific Results 160. pp. 403-417.

Robertson, A.H.F., 1998B. Miocene shallow-water carbonates on the Eratosthenes Seamount, easternmost Mediterranean Sea, in: Robertson, A.H.F., Emeis, K.C., Richter, C., Camerlenghi, A. (Eds.), Proceedings of the Ocean Drilling Program, Scientific Results 160. pp. 419-436.

Robertson, A.H.F., 1998C. Late Miocene Paleoenvironments and tectonic setting of the southern margin of Cyprus and the Eratosthenes Seamount, in: Robertson, A.H.F., Emeis, K.C., Richter, C., Camerlenghi, A. (Eds.), Proceedings of the Ocean Drilling Program, Scientific Results 160. pp. 453-463.

Robertson, A.H.F., 1998D. Formation and destruction of the Eratosthenes Seamount, Eastern Mediterranean Sea, and implications for collisional processes, in: Robertson, A.H.F., Emeis, K.C., Richter, C., Camerlenghi, A. (Eds.), Proceedings of the Ocean Drilling Program, Scientific Results 160. pp. 681-699.

Robertson, A.H.F., 1998E. Mesozoic-Tertiary tectonic evolution of the Easternmost Mediterranean area: integration of marine and land evidence, in: Robertson, A.H.F., Emeis, K.C., Richter, C., Camerlenghi, A. (Eds.), Proceedings of the Ocean Drilling Program, Scientific Results 160. pp. 723-782.

Robertson, A.H.F., 1998F. Tectonic significance of the Eratosthenes Seamount: a continental fragment in the process of collision with a subduction zone in the eastern Mediterranean (Ocean Drilling Program Leg 160). Tectonophysics. 298, 63-82.

Robertson, A.H.F., Dixon, J.E., 1984. Introduction: aspects of the geological evolution of the Eastern Mediterranean, in: Dixon, J.E., Robertson, A.H.F. (Eds.), The Geological evolution of the Eastern Mediterranean. Geological Society Special Publication, 17, Geological Society, London. pp. 1-74.

Robertson, A.H.F., Eaton, S., Follows, E.J., McCallum, J.E., 1991. The role of local tectonics versus global sea-level change in the Neogene evolution of Cyprus margin, in Macdonald, D.I.M (Ed.), Sedimentation, Tectonics and Eustasy: Sea-level changes at active Margins. Special Publication of the International Association of Sedimentologists12. pp. 331-339.

Robertson, A.H.F., Kidd, R.B., Ivanov, M.K., Woodside, J.M., Galindo-Zaldivar, J., Nieto, L., and the Scientific Party of the 1993 'TTR-3' Cruise, 1995. Eratosthenes Seamount: collisional processes in the easternmost Mediterranean in relation to the Plio-Quaternary uplift of southern Cyprus. Terra Nova. 7, 254-264.

Robertson, A.H.F., Parlak, O., Ustaömer, T., 2012. Overview of the Palaeogene-Neogene evolution of Neotethys in the Easter Mediterranean region (southern Turkey, Cyprus, Syria). Petroleum Geoscience. 18, 381-404.

Robertson, A.H.F., Parlak, O., Ustaömer, T., 2013. Late Palaeozoic–Early Cenozoic tectonic development of Southern Turkey and the easternmost Mediterranean region: evidence from the inter-relations of continental and oceanic units, in: Robertson, A.H.F., Parlak, O., Ünlügenç, U.C. (Eds.), Geological Development of Anatolia and the Easternmost Mediterranean Region. Geological Society, London, Special Publications 372. pp. 9-48.

Rögl, F., 1999. Mediterranean and Paratethys facts and hypotheses of an Oligocene to Miocene paleogeography (short overview). Geologica Carpathica. 50. 339-349.

Rösler, A., Perfectti, F., Peña, V., Braga, J.C., 2016. Phylogenetic relationships of Corallinaceae (Corallinales, Rhodophyta): taxonomic implications for reef-building corallines. Journal of Phycology. 52, 412-431.

Rouchy, J.M., Orszag-Sperber, F., Blanc-Valleron, M.M., Pierre, C., Rivière, M., Comborieu-Nebout, N., Panayides, I., 2001. Paleoenvironmental changes at the Messinian-Pliocene boundary in the eastern Mediterranean (southern Cyprus basins): significance of the Messinian Lago-Mare. Sedimentary Geology. 145, 93-117.

Ruttenberg, K.C., 1992. Development of a sequential extraction method for different form of phosphorus in marine sediments. Limnology and Oceanography. 37, 1460–1482.

Ruttenberg, K.C., 2004. The global phosphorus cycle, in: Holland, H.D., Turekian, K.K. (Eds.), Treatise on Geochemistry 8, New York, Elsevier. pp. 585–643.

Ruttenberg, K.C., Ogawa, N.O., Tamburini, F., Briggs, R.A., Colasacco, N.D., Joyce, E., 2009. Improved, high throughput approach for phosphorus speciation in natural sediments via the SEDEX sequential extraction method. Limnology and Oceanography Methods. 7, 319–333.

Schiavinotto, F., 1979. Miogypsina e Lepidocyclina del Monte La Serra (L'Aquila-Appennino Centrale). Geologica Romana. 18, 253-293.

Scoffin, T.P., 1970. The trapping and binding of subtidal carbonate sediments by marine vegetation in Bimini Lagoon, Bahamas. Journal of Sedimentary Petrology. 40, 29–273.

Shevenell, A.E., Kennet, J.P., Lea, D.W., 2004. Middle Miocene Southern Ocean cooling and antarctic cryosphere expansion. Science. 35, 1766-1770.

Skiple, C., Anderson, E., Fürstenau, J., 2012. Seismic interpretation and attribute analysis of the Herodotus and the levantine Basin, offshore Cyprus and Lebanon. Petroleum Science. 18, 433-442.

Sola, F., Braga, J.C., Aguirre, J., 2013. Hooked and tubular coralline algae indicate seagrass beds associated to Mediterranean Messinian reefs (Poniente Basin, Almeria, SE Spain). Palaeogeography, Palaeoclimatology, Palaeoecology. 374, 218–229

Spezzaferri, S., Cita, M.B., McKenzie, J.A., 1998. The Miocene/Pliocene boundary in the Eastern Mediterranean: results from Sites 967 and 969, in: Robertson, A.H.F., Emeis, K.C., Richter, C., Camerlenghi, A. (Eds.), Proceedings of the Ocean Drilling Program, Scientific Results 160. pp. 9-28.

Spezzaferri, S., Tamburini, F., 2007. Paleodepth variations on the Eratosthenes Seamount (Eastern Mediterranean): sea-level changes or subsidence?. eEarth Discuss. 2, 115–132.

Staerker, T.S., 1998. Data report: biostratigraphy of Eocene and Upper Cretaceous chalks from the Eratosthenes Seamount region in the Eastern Mediterranean, in: Robertson, A.H.F., Emeis, K.C., Richter, C., Camerlenghi, A. (Eds.), Proceedings of the Ocean Drilling Program, Scientific Results 160. pp. 395-401.

Steinberg, J., Gvirtzman, Z., Folkman, Y., Garfunkel, Z., 2011. Origin and nature of the rapid late Tertiary fi lling of the Levant Basin. Geology. 39, 355-358.

Lagabrielle, Y., Goddéris, Y., Donnadieu, Y., Malavieille, J., Suarez, M., 2009. The tectonic history of Drake Passage and its possible impacts on global climate. Earth and Planetary Sciences Letters. 279, 197–211.

Stalder, C., Spezzaferri, S., Rüggeberg, A., Pirkenseer, C., Gennari, G., 2014. Late Weichselian deglaciation and early Holocene development of a cold-water coral reef along the Lopphavet shelf (Northern Norway) recorded by benthic foraminifera and ostracoda. Deep-sea Research II. 99, 249–269.

Tan, S.H., 1932. On the genus *Cycloclypeus* Carpenter. Part I, and an appendix on the *Heterostegines* of Tjimanggoe, S. Bantam, Java. Wetenschappelijke Mededeelingen Dienst van den Mijnbouw in Nederlandsch-Indië. 19, 3–194.

Taylforth, J.E., McCay, G.A., Ellam, R., Raffi, I., Kroon, D., Robertson, A.H.F., 2014. Middle Miocene (Langhian) sapropel formation in the easternmost Mediterranean deep-water basin: Evidence from northern Cyprus. Marine and Petroleum Geology. 57, 521-536.

Tomassetti, L., Benedetti, A., Brandano, M., 2016. Middle Eocene seagrass facies from Apennine carbonate platforms (Italy). Sedimentary Geology. 335, 136-149.

Torres-Silva, A.I., Hohenegger, J., Ćorić, S., Briguglio, A., 2017. Biostratigraphy and evolutionary tendencies of Eocene heterostegines in Western and Central Cuba based on morphometric analyses. Palaios. 32, 44-60.

Tosquella, J., González-Regalado, M.L., Ruiz, F., Baceta, J.I., 2001. El género *Heterostegina* (Nummulitidae, Foraminifera) en el Miocene superior del SO de Espaňa. Geobios. 34, 279-290.

Tyrrell, T., 1999. The relative influence of nitrogen and phosphorus on ocean primary production. Nature. 400, 525–531.

Van der Vlerk, I.M., 1959. Modifications de l'ontogénèse pendant l'évolution des Lépidocyclines (Foraminifères). Bulletin de la Société Géologique de France, Notes et Mémoires, Série 7. 1, 669-673.

Van der Vlerk, I.M., 1963. Biometric research on *Lepidocyclina*. Micropaleontology. 9, 425–426.

Van Vessem, E.J., 1978. Study of Lepidocyclinidae from South-East Asia, particularly from Java and Borneo. Utrecht Micropalaeontological Bullettin. 19, 1-163.

Vennin, E., Rouchy, J.M., Chaix, C., Blanc-Valleron, M.M., Caruso, A., Rommevau, V., 2004. Paleoecological constrains on reef-coral morphologies in the Tortonian-early Messinian of the Lorca Basin, SE Spain. Palaeogeography, Palaeoclimatology, Palaeoecology. 213, 163-185.

Verrubbi, V., Schiavinotto, F., 2005. *Miogypsina globulina* (Michelotti) from Samatzai section (Lower Miocene - Southern Sardinia). Bollettino della Società Paleontologica Italiana. 44, 203-209.

Woelkerling, W.J., 1988. The coralline red algae: an analysis of the genera and subfamilies of nongeniculate Corallinaceae. Oxford University Press, New York.

Whiting, B.M., 1998. Subsidence record of early stage continental collision, Eratosthenes Platform (Sites 966 and 967), in: Robertson, A.H.F., Emeis, K.C., Richter, C., Camerlenghi, A. (Eds.), Proceedings of the Ocean Drilling Program, Scientific Results 160. pp. 509-515.

Yılmaz, Y., 1993. New evidence and model on the evolution of the southeast Anatolian orogen. Geological Society of America Bulletin. 105, 251-271.

Zachos, J., Pagani, M., Sloan, L., Thomas, E., Billups, K., 2001. Trends, Rhythms, and Aberrations in Global Climate 65 Ma to Present. Science. 292, 686-693.

Table Caption

Table 1: Average composition of the skeletal assemblage and Dunham classification of the facies of Hole 966F. The slash bar between rudstone and boundstone is used since, due to the limited size of the core and the poor recovery, it is impossible to check whether or not there are bioconstructions in the facies.

Cores	26R-1 to 20R	19R-3	19R-2 to 16R-2	16R-1 to 15R-1	14R-1 to 11R	10R to 7R-1	7R-1
Facies	LBF and echinoids	Rhodolith and coral	Coralline algal and *Heterostegina*	Rhodolith and coral	Coral-reef	Mollusc and benthic foraminifer	Mollusc and ostracod
Dunham classification	Grainstone	Rudstone	Wackestone to packstone	Rudstone	Rudstone/ boundstone	Grainstone to wackestone	Packstone
Coralline algae	14%	63.5%	63%	67%	32.5%	16%	0%
Corals	0%	12%	0%	21%	38%	14.5%	0%
Benthic foraminifera	51.5%	17%	29%	11%	21.5%	43%	15%
Planktonic foraminifera	10%	0%	1%	0%	0%	0.5%	0%
Echinoids	21.5%	7%	3.5%	0.5%	3%	4%	0%
Molluscs	1.5%	0.5%	2%	0%	4.5%	18%	17%
Ostracods	0%	0%	0.5%	0%	0%	2%	68%
Bryozoans	1%	0%	0.5%	0.5%	0%	1.5%	0%
Others	0.5%	0%	0.5%	0%	0.5%	0.5%	0%

Highlights

The stratigraphy of Miocene carbonates of the Eratosthenes is revised

Foraminifera dominate the early Miocene, algae the middle and corals the late Miocene

Lepidocyclinids and miogypsinids extinction occurs at the end of the early Miocene

CT-scan is suitable for study microfossils still embedded into the rock

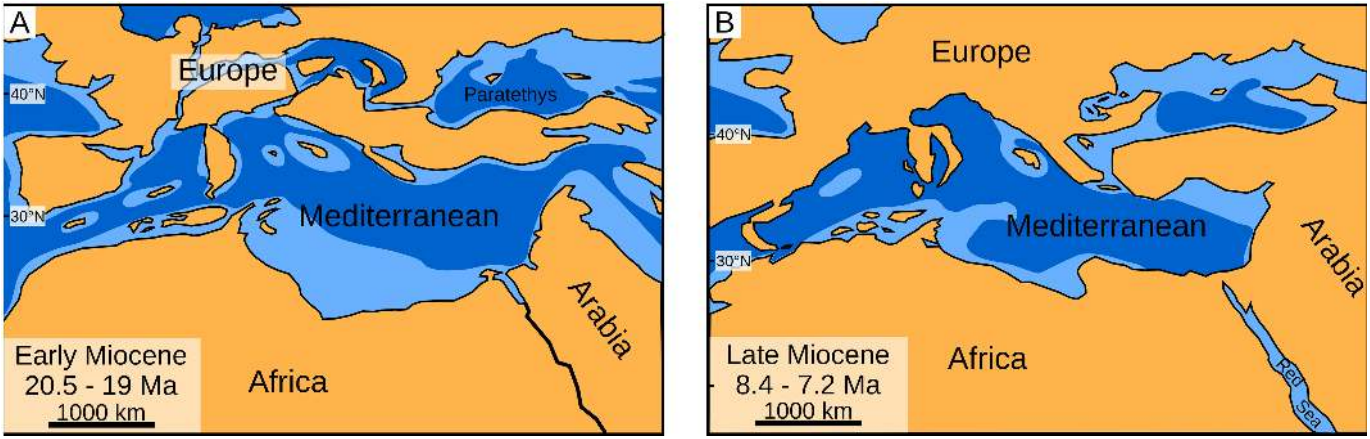
A
Europe
Paratethys
40°N
30°N
Mediterranean
Arabia
Early Miocene
20.5 - 19 Ma
1000 km
Africa
B
Europe
40°N
30°N
Mediterranean
Arabia
Late Miocene
8.4 - 7.2 Ma
1000 km
Africa
Red Sea

Figure 1

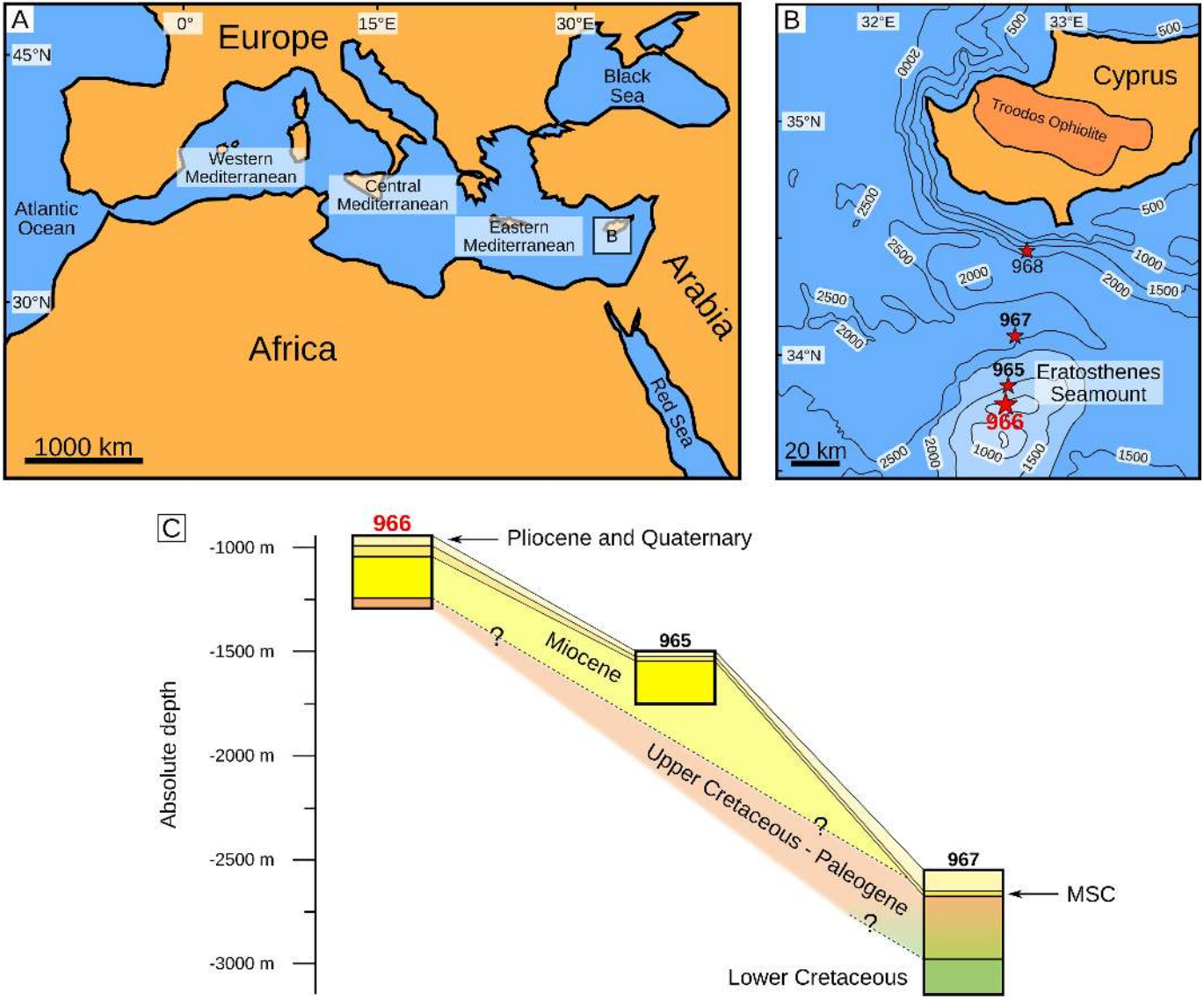
A
0°
15°E
30°E
45°N
Europe
Black Sea
Western Mediterranean
Central Mediterranean
Eastern Mediterranean
B
Atlantic Ocean
30°N
Africa
Arabia
Red Sea
1000 km
B
32°E
33°E
35°N
34°N
Cyprus
Troodos Ophiolite
968
967
965
966
Eratosthenes Seamount
20 km
C
966
965
967
Pliocene and Quaternary
Miocene
Upper Cretaceous - Paleogene
Lower Cretaceous
MSC
Absolute depth
-1000 m
-1500 m
-2000 m
-2500 m
-3000 m

Figure 2

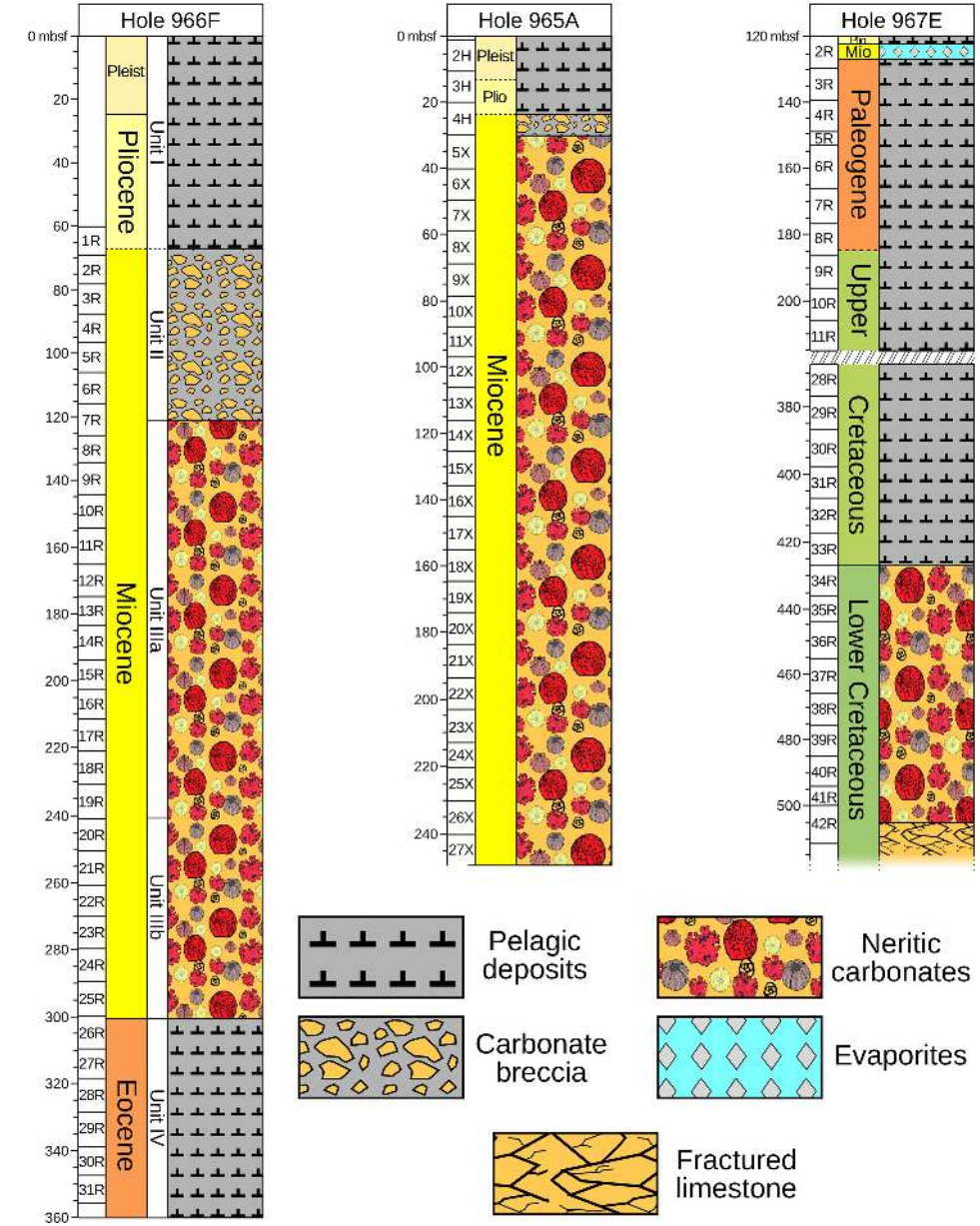
Hole 966F
0 mbsf
Pleist
Pliocene
Miocene
Eocene
Unit I
Unit II
Unit IIIa
Unit IIIb
Unit IV
1R
2R
3R
4R
5R
6R
7R
8R
9R
10R
11R
12R
13R
14R
15R
16R
17R
18R
19R
20R
21R
22R
23R
24R
25R
26R
27R
28R
29R
30R
31R
0
20
40
60
80
100
120
140
160
180
200
220
240
260
280
300
320
340
360
Hole 965A
0 mbsf
Pleist
Plio
Miocene
2H
3H
4H
5X
6X
7X
8X
9X
10X
11X
12X
13X
14X
15X
16X
17X
18X
19X
20X
21X
22X
23X
24X
25X
26X
27X
0
20
40
60
80
100
120
140
160
180
200
220
240
Hole 967E
120 mbsf
Pli
Mio
Paleogene
Upper Cretaceous
Lower Cretaceous
2R
3R
4R
5R
6R
7R
8R
9R
10R
11R
28R
29R
30R
31R
32R
33R
34R
35R
36R
37R
38R
39R
40R
41R
42R
120
140
160
180
200
380
400
420
440
460
480
500
Pelagic deposits
Carbonate breccia
Fractured limestone
Neritic carbonates
Evaporites

Figure 3

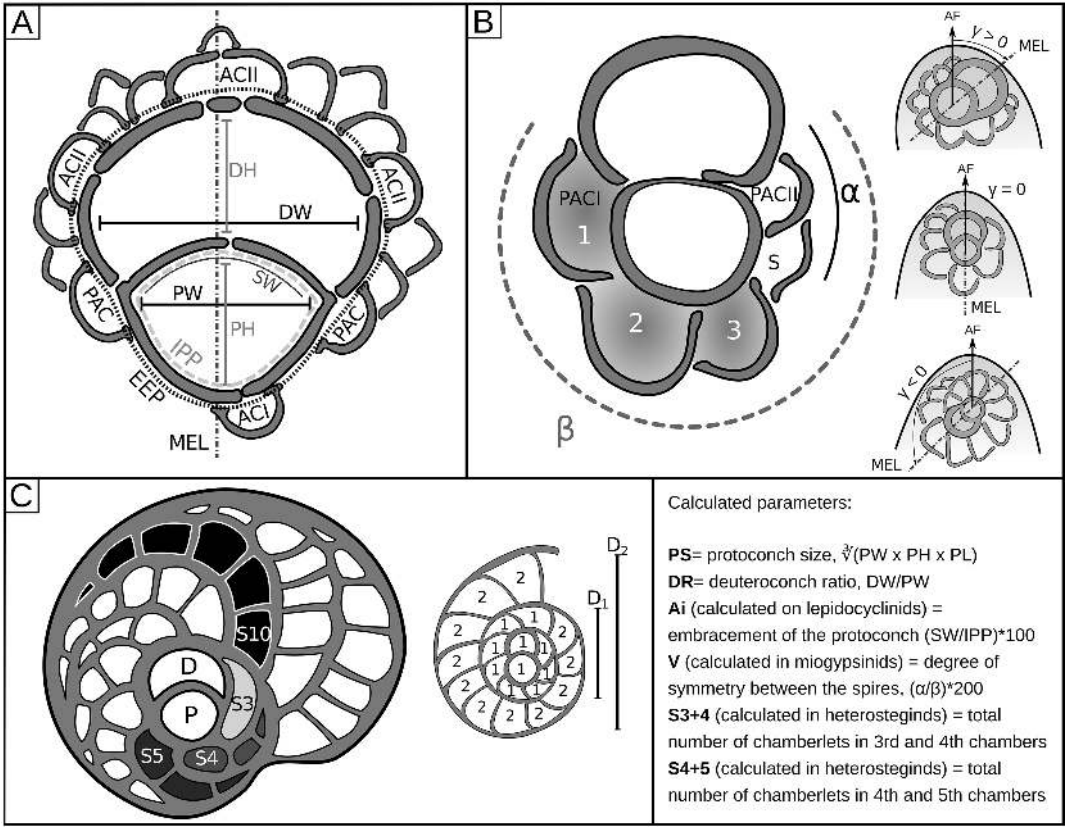
A
ACII
ACII
ACII
DH
DW
PW
SW
PH
IPP
PAC
PAC
EEP
ACI
MEL
B
PACI
PACII
α
1
2
3
S
β
AF
γ > 0
MEL
AF
γ = 0
MEL
AF
γ < 0
MEL
C
S10
D
P
S3
S5
S4
2
1
D2
D1
Calculated parameters:
PS= protoconch size, ∛(PW x PH x PL)
DR= deuteroconch ratio, DW/PW
Ai (calculated on lepidocyclinids) = embracement of the protoconch (SW/IPP)*100
V (calculated in miogypsinids) = degree of symmetry between the spires. (α/β)*200
S3+4 (calculated in heterosteginds) = total number of chamberlets in 3rd and 4th chambers
S4+5 (calculated in heterosteginds) = total number of chamberlets in 4th and 5th chambers

Figure 4

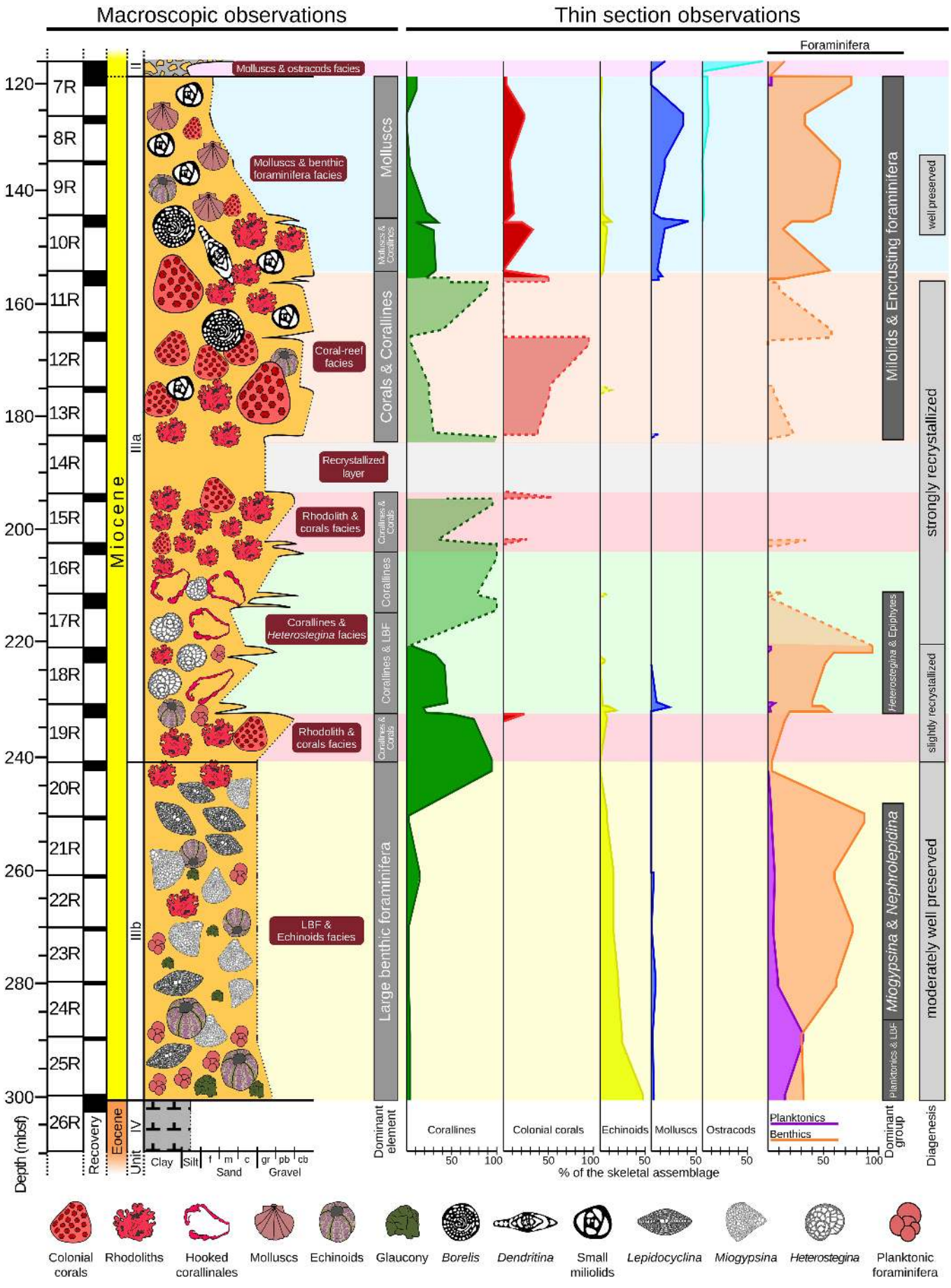
Macroscopic observations
Thin section observations
Foraminifera
Molluscs & ostracods facies
Molluscs & benthic foraminifera facies
Coral-reef facies
Recrystallized layer
Rhodolith & corals facies
Corallines & Heterostegina facies
Rhodolith & corals facies
LBF & Echinoids facies
Molluscs
Molluscs & Corallines
Corals & Corallines
Corallines & Corals
Corallines
Corallines & LBF
Corallines & Corals
Large benthic foraminifera
Miliolids & Encrusting foraminifera
Heterostegina & Epiphytes
Miogypsina & Nephrolepidina
Planktonics & LUK
well preserved
strongly recrystallized
slightly recrystallized
moderately well preserved
Miocene
Eocene
IIIa
IIIb
II
IV
7R
8R
9R
10R
11R
12R
13R
14R
15R
16R
17R
18R
19R
20R
21R
22R
23R
24R
25R
26R
120
140
160
180
200
220
240
260
280
300
Depth (mbsf)
Recovery
Unit
Clay
Silt
Sand
Gravel
Dominant element
Corallines
Colonial corals
Echinoids
Molluscs
Ostracods
% of the skeletal assemblage
Planktonics
Benthics
Dominant group
Diagenesis
Colonial corals
Rhodoliths
Hooked corallinales
Molluscs
Echinoids
Glaucony
Borelis
Dendritina
Small miliolids
Lepidocyclina
Miogypsina
Heterostegina
Planktonic foraminifera

Figure 5

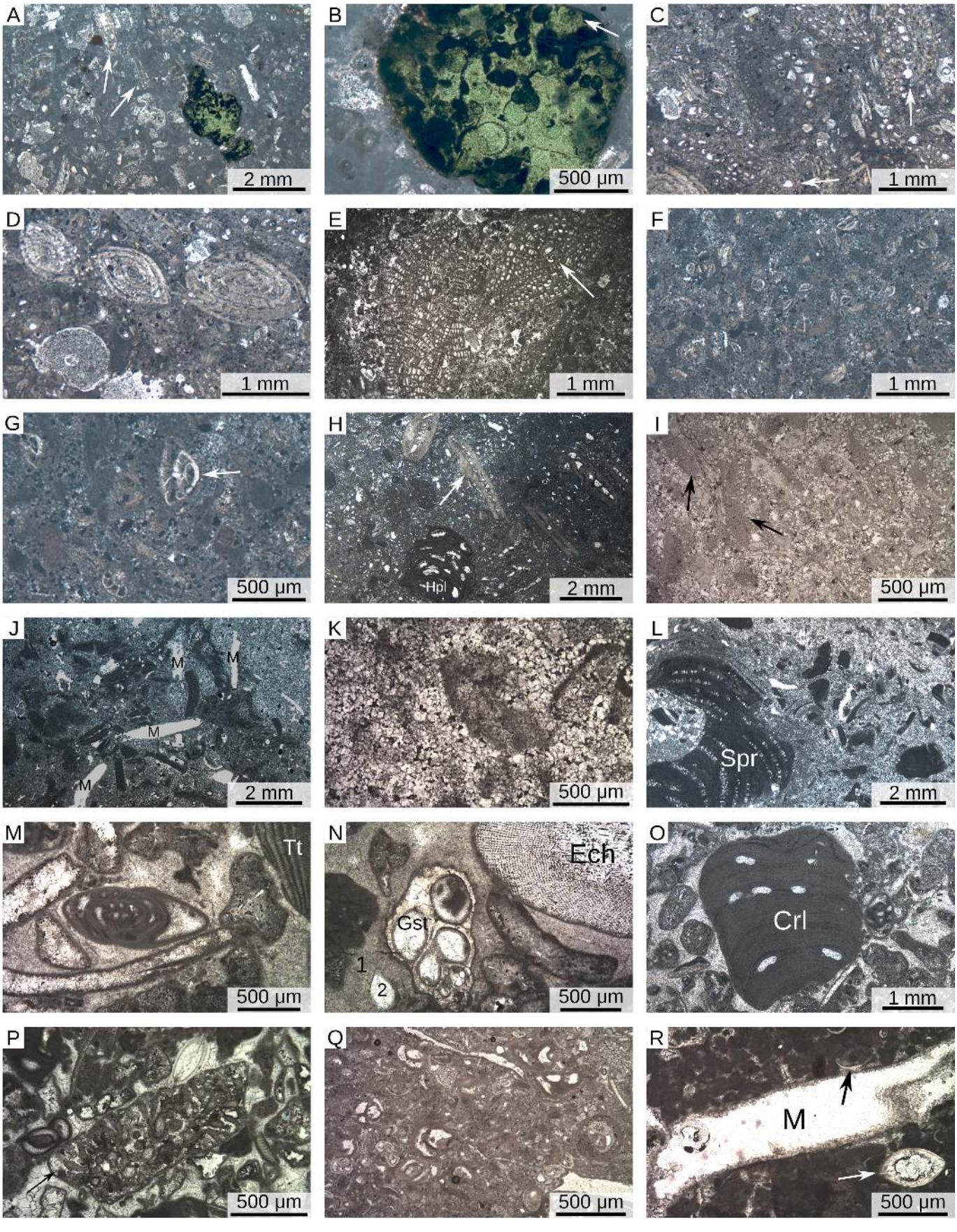
A
2 mm
B
500 µm
C
1 mm
D
1 mm
E
1 mm
F
1 mm
G
500 µm
H
Hpl
2 mm
I
500 µm
J
M
M
M
M
2 mm
K
500 µm
L
Spr
2 mm
M
Tt
500 µm
N
Ech
Gst
1
2
500 µm
O
Crl
1 mm
P
500 µm
Q
500 µm
R
M
500 µm

Figure 6

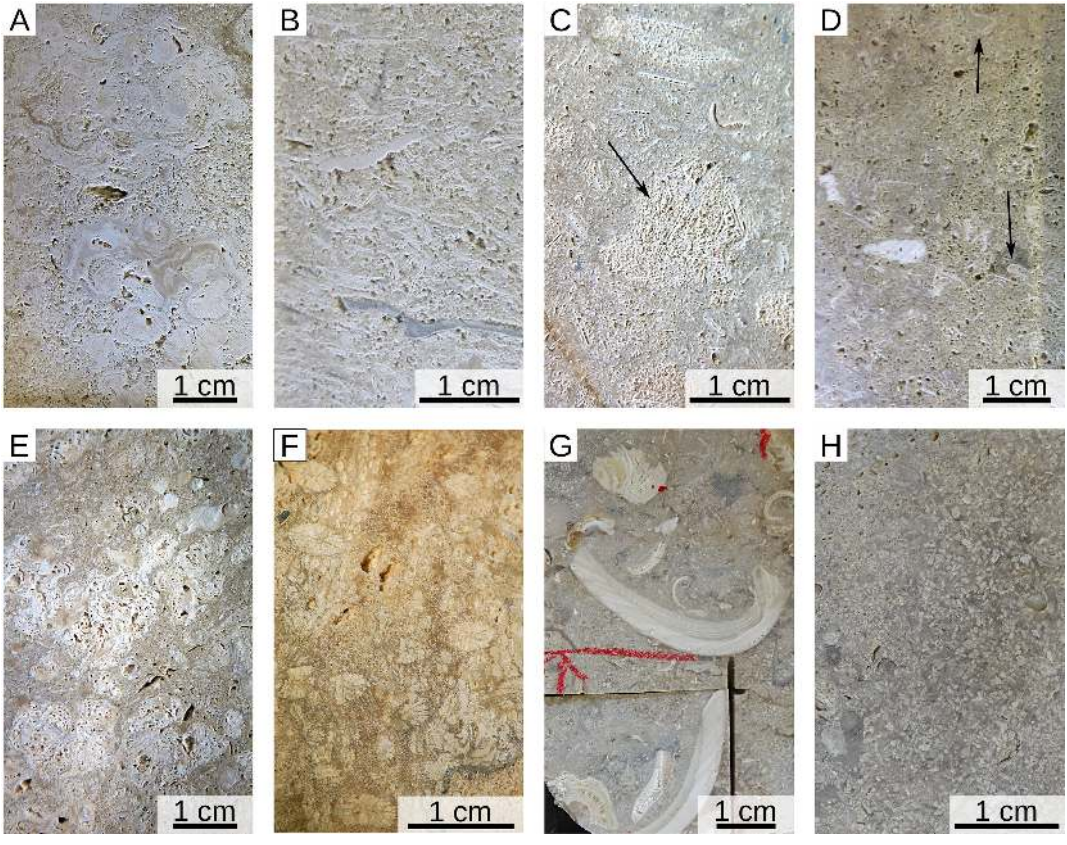

Figure 7

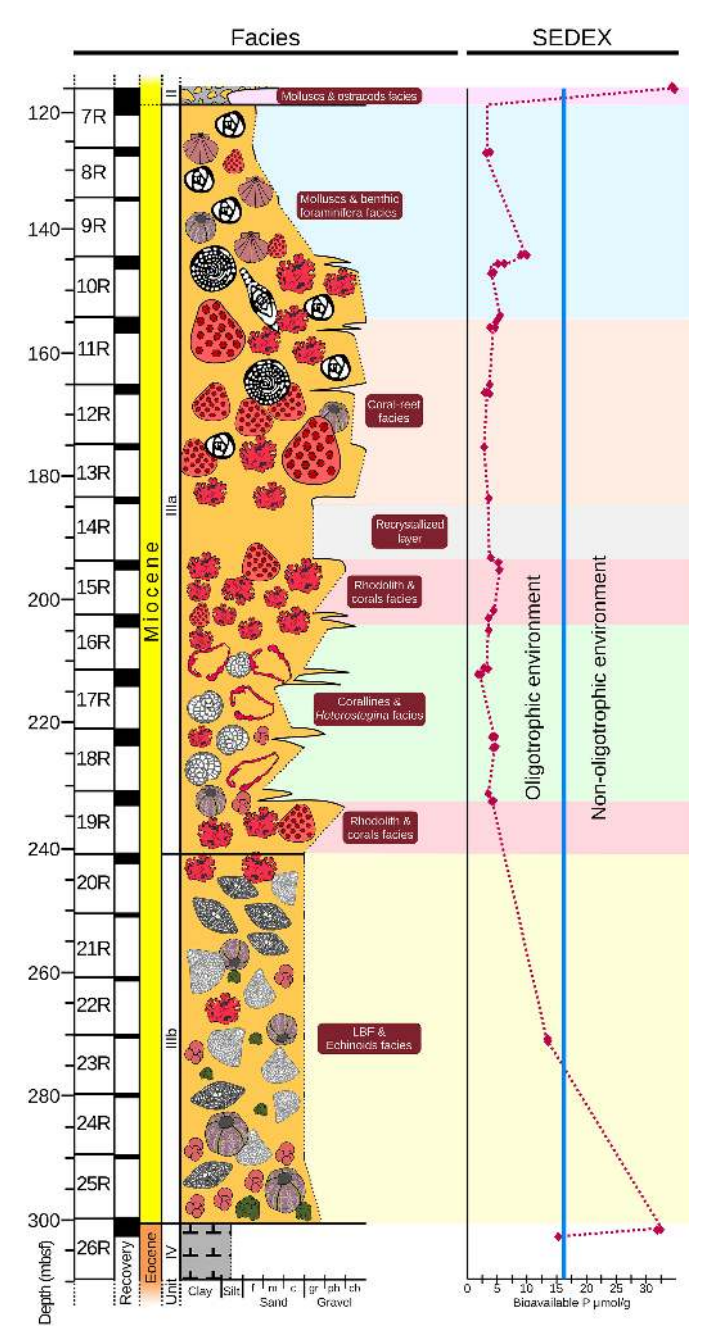
Facies
SEDEX
Molluscs & ostracods facies
Molluscs & benthic foraminifera facies
Coral-reef facies
Recrystalized layer
Rhodolith & corals facies
Corallines & Heterostegina facies
Rhodolith & corals facies
LBF & Echinoids facies
Miocene
Eocene
II
IIIa
IIIb
IV
Unit
Recovery
Depth (mbsf)
7R
8R
9R
10R
11R
12R
13R
14R
15R
16R
17R
18R
19R
20R
21R
22R
23R
24R
25R
26R
120
140
160
180
200
220
240
260
280
300
Clay
Silt
Sand
Gravel
Oligotrophic environment
Non-oligotrophic environment
0
5
10
15
20
25
30
Bioavailable P µmol/g

Figure 8

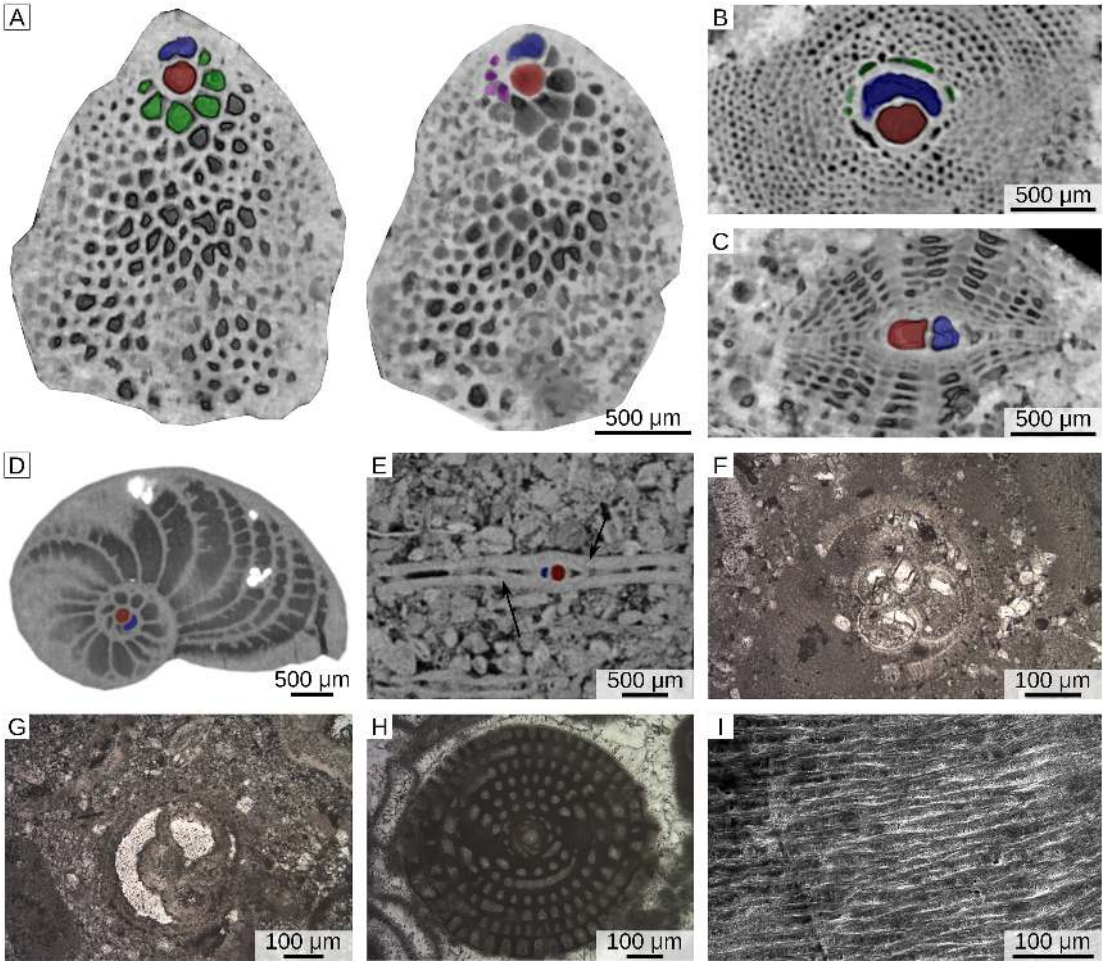
A
500 µm
B
500 µm
C
500 µm
D
500 µm
E
500 µm
F
100 µm
G
100 µm
H
100 µm
I
100 µm

Figure 9

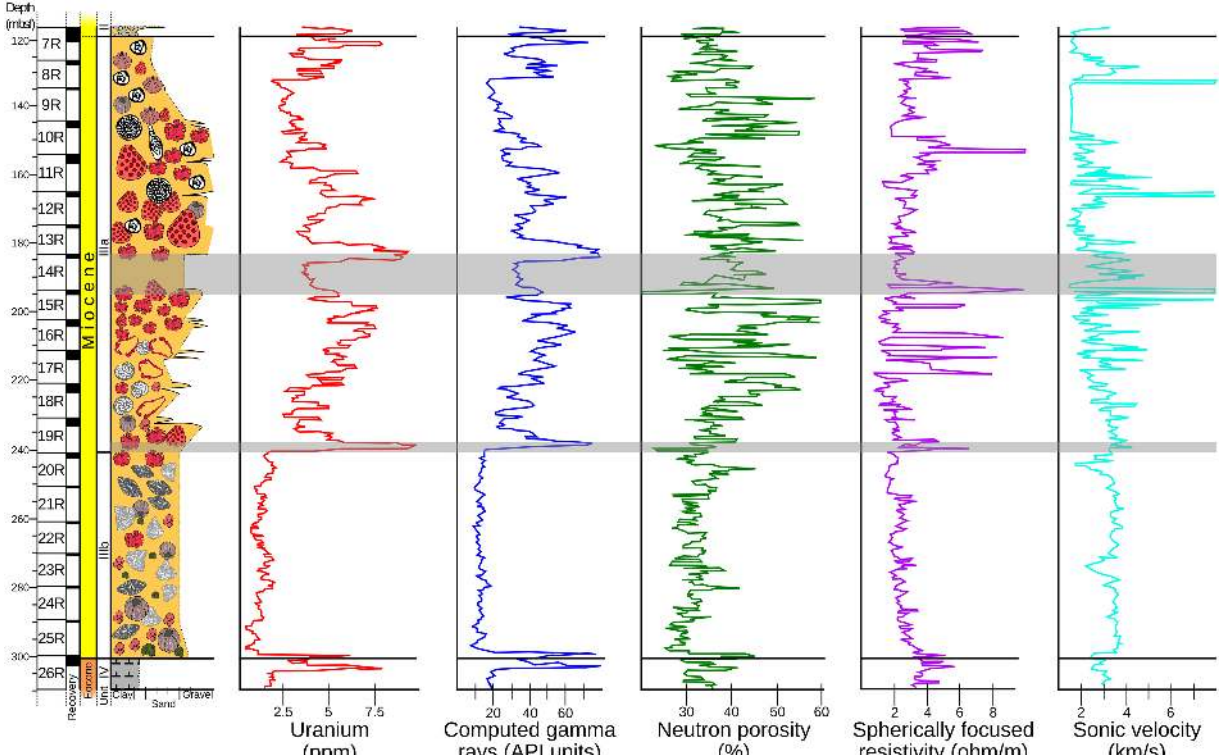
Depth (mbsf)
120
140
160
180
200
220
240
260
280
300
7R
8R
9R
10R
11R
12R
13R
14R
15R
16R
17R
18R
19R
20R
21R
22R
23R
24R
25R
26R
Miocene
IIIa
IIIb
Recovery
Hiatus
Unit IV
Clay
Sand
Gravel
2.5
5
7.5
Uranium (ppm)
20
40
60
Computed gamma rays (API units)
30
40
50
60
Neutron porosity (%)
2
4
6
8
Spherically focused resistivity (ohm/m)
2
4
6
Sonic velocity (km/s)

Figure 10

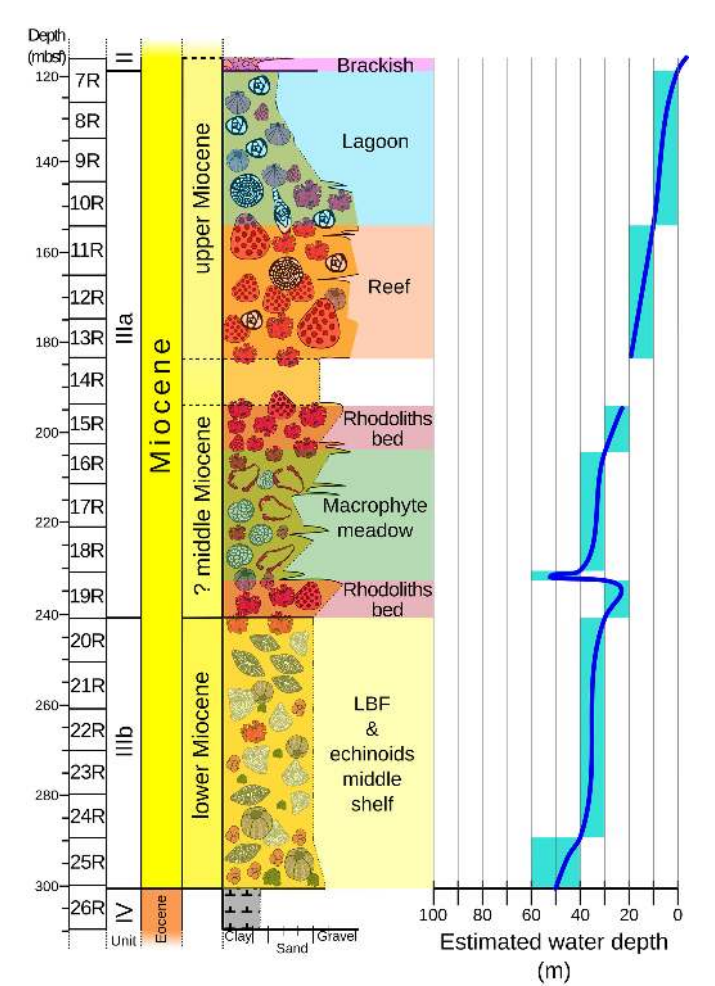
Depth (mbsf)
II
IIIa
IIIb
IV
Miocene
upper Miocene
? middle Miocene
lower Miocene
Eocene
Unit
7R
8R
9R
10R
11R
12R
13R
14R
15R
16R
17R
18R
19R
20R
21R
22R
23R
24R
25R
26R
120
140
160
180
200
220
240
260
280
300
Brackish
Lagoon
Reef
Rhodoliths bed
Macrophyte meadow
Rhodoliths bed
LBF & echinoids middle shelf
Clay
Sand
Gravel
100
80
60
40
20
0
Estimated water depth (m)

Figure 11

A

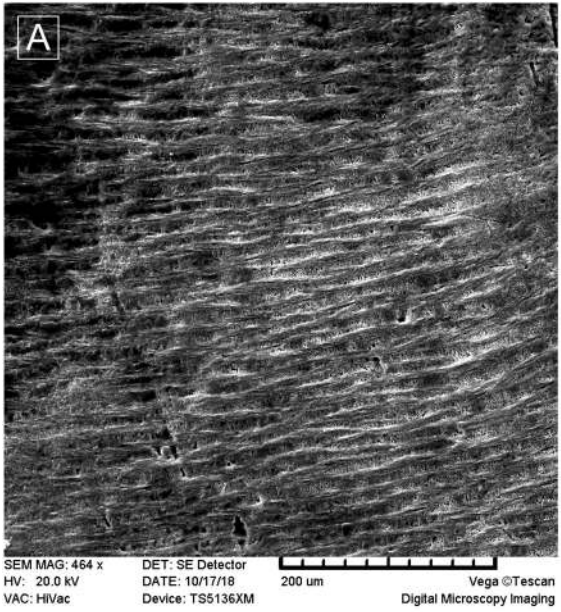

B

10R2-60-62a		
element	value (ppm)	± σ
Ca	385,630.0	1917.7
Mg	269.2	2.1
Sr	1348.0	4.5
Fe	33.0	0.2
Mn	1.1	0.2

C

Sample	Type	$^{87}Sr/^{86}Sr$ corrected value	± 2σ	Preferred age (Ma)
10R2-60-62a	aragonitic shell	0.708925	0.000005	8.40
10R2-60-62b	cement	0.708932	0.000005	8.00

D

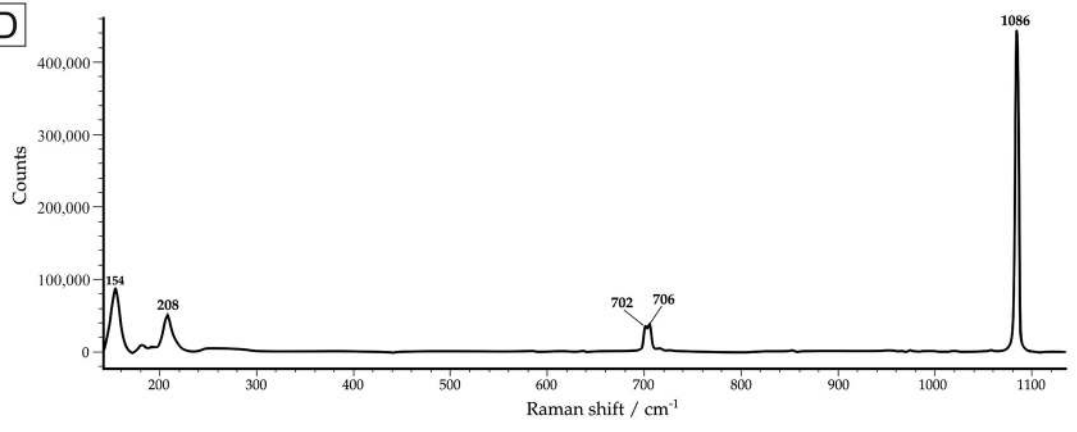

Figure 12